Coating processes towards selective laser sintering of energetic material composites

By

Zetu Jiba

Dissertation submitted in partial fulfilment of the requirements for the degree

Master of Science (Applied Science) Chemical Technology

Department of Chemical Engineering.

Faculty of Engineering, Built Environment and Information Technology,

University of Pretoria

Pretoria, South Africa

2019

Declaration

I, Zetu Jiba, student number 17397678, hereby declare that this research is my original work and that to the best of my knowledge, it has not been previously in its entirety or in part been submitted and is not currently being submitted either in whole or in part at any other university for a degree or diploma, and that all references are acknowledged.

Signature

Date

Coating processes towards selective laser sintering of energetic material composites

Student: Zetu Jiba

Supervisor: Prof. Walter W. Focke

Degree: Masters (Chemical Technology)

Department of Chemical Engineering

University of Pretoria

Abstract

This research aims to contribute to the safe methodology for additive manufacturing (AM) of energetic materials. Coating formulation processes were investigated to find a suitable method that may enable selective laser sintering (SLS) as the safe method for fabrication of high explosive (HE) compositions. For safety and convenience reasons, the concept demonstration was conducted using inert explosive simulants with properties quasi-similar to the real HE. Coating processes for simulant RDX-based microparticles by means of PCL and 3,4,5-trimethoxybenzaldehyde (as TNT simulant) are reported. These processes were evaluated for uniformity of coating the HE inert simulant particles with binder materials to facilitate the SLS as the adequate binding and fabrication method. The critical constraints being the coating effectiveness required, spherical particle morphology, micron size range (>20 μm) and a good powder deposition and flow, and performance under SLS to make the method applicable for HEs.

Of the coating processes investigated, suspension system and single emulsion methods gave required particle near spherical morphology, size and uniform coating. The suspension process appears to be suitable for the SLS of HE mocks and potential formulation methods for active HE composites. The density was estimated to be comparable with the current HE compositions and plastic bonded explosives (PBXs) such as C4 and PE4, produced from traditional methods.

The formulation method developed and the understanding of the science behind the processes paves the way toward safe SLS of the active HE compositions and may open avenues for further research and development of munitions of the future.

Keywords: *Coating processes; Energetic Materials; Simulants; Mock explosives; Additive manufacturing; Selective Laser Sintering*

Acknowledgements

To my supervisor, Prof. Walter Focke. Your zest for good research output and your candid character is contagious. You may not remember now, but there's a long phrase that you gave me that kept me going through this study *"You are the master of your work and you must treat this study like your baby, seek assistance and support from different areas you can get to ensure that the baby is well taken care of"*. Your words echoed in my mind and helped me to be proactive. Thank you for that Walter.

To my co-supervisor, Mr Lonji Kalombo. Thank you for always encouraging me to go back to the basics of science so I can understand the mechanisms and dynamics of this study.

To CSIR, Defence Peace Safety and Security (DPSS-LS), I cannot thank you enough for all the support and funding for this study. My DPSS-LS former group, thanks for listening to my *gobbledygook* and your willingness to offer feedback. A special thank you to Dr Tleyane Sono for his technical advices throughout this journey. I will always keep the phrase "*make it hard for them not to follow*" in mind.

I would like to extend a word of appreciation to the University of Pretoria microscopy laboratory group for assisting me with measurements of my samples. To Prof. Walter's students; Shasha Guo and Robert for assisting me with microscope bookings and letting me use your schedules and to Marnes Grobler for always willing to assist with the laser system set-up. And to extend our gratitude to Paul Sonnendecker in Chemical Engineering, University of Pretoria, for assisting with the solar system SLS test.

Lastly, to my mother who would not understand a thing I am talking about when I am frantic with worry and whining about my studies and would just tell me "*You're a strong girl and you are never a quitter, you'll figure it out*". Your tough words and love kept me going and I am truly grateful to have you in my life.

Table of Contents

Contents

Table of Figures

List of tables

Abbreviations

ABC	acrylonitrile butadiene styrene
AFM	Atomic Force Microscopy
AM	Additive Manufacturing
CSIR	Council for Scientific and Industrial Research
DL-TTA	DL-Tartaric acid
DSC	Differential Scanning Calorimetry
EM	Energetic Materials
FTIR	Fourier-transform Infrared
HEMs	High Energetic Materials
HIPS	high impact polystyrene
KBT	Potassium bitartrate
KBT	Potassium Bitartrate
MP	Melting Point
PCL	Polycaprolactone
PLA	polylactic acid
PMMA	Polymethylmethacrylate
PVA	polyvinyl alcohol
RDX	Hexogen/Cyclotrimethylenetrinitramine
SEM	Scanning Electron Microscopy
SLM	Selective Laser Manufacturing
SLS	Selective Laser Sintering
T_g	Glass Transition
TNT	2,4,6-Trinitrotoluene
UP	University of Pretoria

1. Introduction

Additive manufacturing (AM) technologies are maturing and allowing effective manufacturing of components, including those of energetic material devices. Conversely, technology advances in AM may also enable more sophisticated fabrication of improvised explosive devices that are hard to detect. Stakeholders within the defence research and development sector need to be aware of this potential threat and strive to develop counter solutions. AM is a broad-spectrum term that includes several technologies that can create 3D objects by adding material layer-by-layer. The benefits of the AM of materials include rapid prototyping, control over the material composition, and cost-effective manufacture of short product runs. The AM processing of energetic materials allows structuring of the material at the mesoscale, something that is challenging to achieve with conventional methods. The material composition can be controlled, the particles can be manipulated from micro to mesoscale and manufactured for unique structures in theatre [1-3].

AM, commonly referred to as three-dimensional (3D) printing, is a non-conventional manufacturing process by which materials are added layer-by-layer to form a desired solid geometry instead of subtracted. AM processes are not subject to the constraints associated with traditional manufacturing methods, and they provide significant opportunities for the design of novel geometries and complex internal structures to enhance component properties, such as the strength-to-weight ratio and cooling, in comparison to traditional manufacturing methods [4]. With current additive technologies, functional polymer and other material parts can be built directly from computer models or from measurements of existing components to be re-engineered, as opposed to the early days of rapid prototyping, and therefore bypass traditional manufacturing processes such as cutting, milling, and grinding. Benefits of AM, shown in Figure 1, include (1) new designs not possible using conventional subtractive technology; (2) dramatic savings in time, materials, waste, energy, and other costs in producing new components; (3) significant reductions in environmental impact; and (4) faster time to market for products.

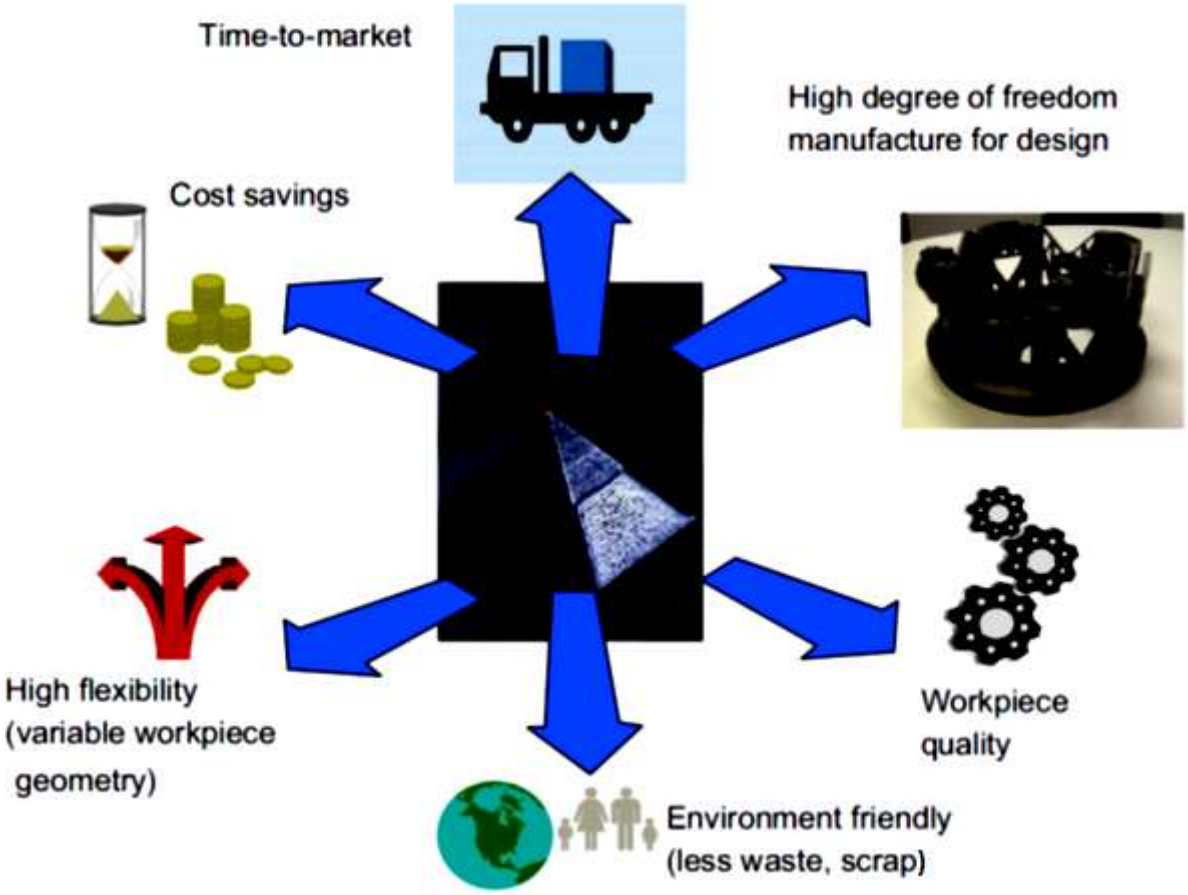

Figure 1: Benefits of AM [5].

1.1 Subject

The rapid development in the technology of additive manufacture will also affect the field of explosive materials. It has to be accepted that this technology will in future be available to defence forces and adverse insurgent elements alike. It is therefore imperative that proactive research is executed to gauge the potential application of this technology and processes that can be used for energetic material manufacturing. Understanding these processes will enable further research on the effects of emerging high explosive compositions and devices to provide protection solutions and countermeasures against such threats. Other advantages of AM of explosive devices include:

- a need for precision placement of materials while minimising wastage,
- to obtain unique structures for warheads which are not obtainable by traditional ways,
- to have control of composition as gradients can produce unique explosive effects, for improved insensitivity,
- reduced time between design and manufacturing, and

- cost saving and material control and from the logistics point of view, this would be a great application for the military as the munitions could be prepared in the theatre of operations instead [3-10].

Currently, the traditional manufacturing methods for explosive devices are limited to production via cast-cure, melt-cast, and pressed powder. High explosives, such as RDX-based composite materials are currently limited to production via the pressed powder method or castable mixtures which require further processing for unusual shapes and which introduce sensitivity and safety issues in the manufacturing process. Furthermore, the processes are difficult and costly to update large-scale preparation plants [1]. The pressed powders process includes explosive powder materials, wax or polymer binder and solvent producing polymer/plastic bonded explosives (PBXs), whereby the energetic particles are first coated with a binder.

PBXs have been commonly used in both military and industry because of their improved safety, enhanced mechanical properties and reduced vulnerability during storage and transportation [6-11]. There is, however, an increasing need to improve the manufacturing method for high explosives (HEs) to achieve unique shapes that can be produced for different unique detonation and explosion effects, manipulation of particle sizes from micro to mesoscales. The ability of other AM methods such as fused deposition method, inkjet printing and binder jetting has been demonstrated on pyrotechnics and propellants [3,4]. Components compatible with high explosives have been manufactured through AM methods in theatre as containers for holding the explosive charges [11].

Researchers have attempted the 3D printing process on TNT, a high explosive material, but difficulties in controlling its behaviour and safety issues that arise during and after the process still remains a concern . As such, 3D printing studies of a mock TNT material was executed to try control and tailor internal structures for a new explosive form. Gash studied and developed the methodology to synthesise plastic-bonded high active explosive components for direct ink-write AM process, whereby the product consisted of 94% explosive crystal material by weight bonded together as agglomerate by 6% thermoplastic polymer [15].

Selective laser sintering (SLS) is another AM approach of interest, envisaged for manufacturing energetic material devices. It uses a laser to sinter powdered plastic material into a solid structure based on a 3D model. The laser is the source of heat for the process and its power, beam diameter,

and intensity profile on the surface of the work piece affect build rates, microstructure, and, through the microstructure, component properties [4].

This technique is unprecedented for energetic materials. SLS offers the freedom to quickly build complex parts that are more durable and provide better functionality over other AM processes. It a dry powder deposition method, whereby the particles are fused together by the laser beam energy.

- Parts printed are very accurate and precise compared to other processes,
- No support structures are required due to the powder bed supporting the part,
- No post curing is required, and the process time is fast.
- Pre-processing is paramount to ensure safety during the manufacturing process.
- Prior to sintering with the laser beam, the absorbing material (binder particles) are not completely melted but instead the temperature is raised to just above the glass transition temperature (amorphous polymers) or just below the melting temperature (semi-crystalline polymers/binders) where the material becomes soft and rubber
- The laser has a fast scanning speed which can be adjusted and reduces printing time,
- There is no risk of clogging such as with the nozzles included in other processes,
- Larger parts can be printed due to the larger build envelope.

The fundamentals of selective laser sintering (SLS) are illustrated in Figure 2. This process utilises an x-y-plane scanning laser beam (usually a carbon dioxide laser) to selectively melt patterns out of a bed of polymer or any material particles and, in doing so, to build the 3D part, layer by layer [12]. The newly formed layer cools and solidifes through conduction and joins with the previously formed layer. After the layer has been sintered. For an automated SLS system, the supporting platform is lowered (movement in the z-direction) and a new layer of fresh powder is applied. Powder application is usually done by a roller that rotates anticlockwise to the direction of travel to evenly distribute the powder [11]. The process occurs much faster at higher temperatures which is why sintering involves heating a powder. Sintering is different from melting in that the materials never reach a liquid phase during the sintering process [13].

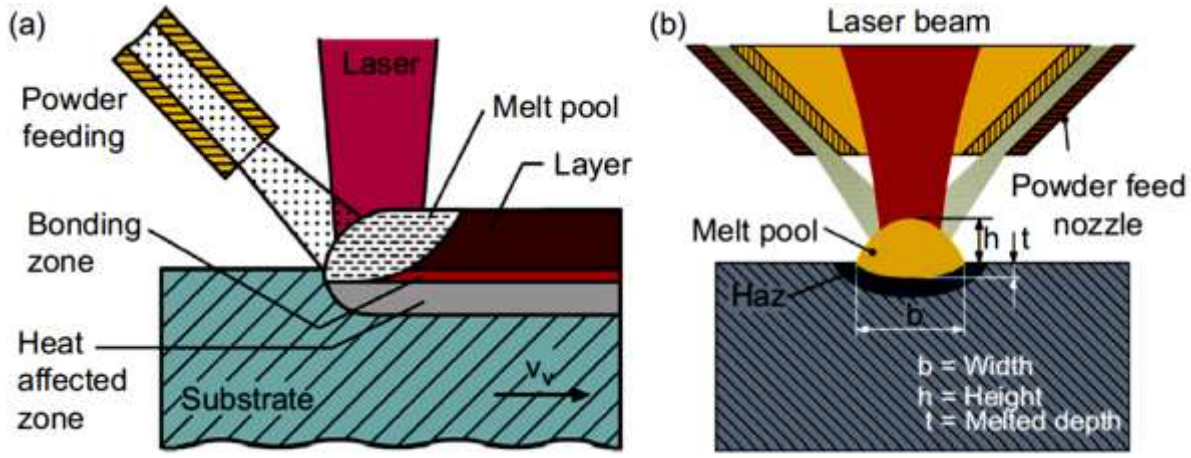

Figure 2: Schematic of the automated powder bed SLS process with (off-axis powderdeposition and (b) continuous coaxial powder feeding, HAZ Heat affected zone [14,15].

However, SLS operation is complicated as many build variables need to be decided, hence pre-processing of the powder is required. The absorption and scattering effect by the material particles must be taken into consideration. The disadvantages are that the accuracy is limited by the size of particles of the material, oxidation needs to be avoided by executing the process in an inert gas atmosphere and for the process to occur at constant temperature near the melting point [16].

The most important powder property is depositability, which depends on the size and shape of the particles. Deposition can be performed with the powder in either a dry or wet state, but the acceptable particle sizes are different for each deposition process. Particles that are 20-100 microns and larger are preferably deposited in the dry state, while particles smaller than 5 microns can be deposited in either the dry or wet state [17]. Fine powders (~1 micron) tend to agglomerate due to van der Waal's forces and moisture effects [18], so mechanical spreading can be problematic. Fine powders can be deposited in a dry state, but only as a low volume percentage in a predominantly larger diameter powder formulation or as bound agglomerations of smaller particles [19] but can affect sinterability. Fine particles can instead be deposited as a slurry when the particle size is less than about 5 microns [17]. The spherical powders are preferred for dry deposition because they tend to flow better [2] and have low internal friction [19]. Faceted or anisotropic powders have much more frequent inter-particle contact than spherical powders, and the increased internal friction lowers the spreadability of powders with these particle shapes, but may increase the packing ratio [19]. The particle size affects design parameters of both the printing process and the final part [20].

It goes without saying that selected desensitisers/sensitizers should have very high absorbance at around the peak of the laser wavelength band used and should be inexpensive in order to make the procedure cost-effective. Two important things need to be considered in the formulation and preparation of samples namely; negligible conglomerations of either the HE particles or the binder particles, and uniformity of the coating of the particles on the surface of the HE simulant. For the latter, the binder particles should be as fine as possible [21].

This dissertation reports on investigation into coating processes of energetic materials for potential use in one of the additive manufacturing technique, selective laser sintering.The energetic material simulants and coating processes investigated are similar to those reported in the literature [22-27]. The selection of the RDX inert simulant was primarily constrained by the solubility in the solvents used and thermal attributes compared to RDX, with quasi-comparable physical properties. A binder, with a low melting point but fast solidification properties and with a very high IR absorbance at the peak of the laser wavelength band, in contrast to the RDX simulant, was used [27-28]. The proposed formulation method developed, may in future enable safe additive preparation of non-cast HE compositions, and it furthers the research and development of novel munitions.

1.2 Problem Statement

A survey of other possible melt-cure polymer binders suitable for use in energetic material formulations for AM technologies was conducted [1]. Polymer bonding studies, particle size effects and laser ignition studies on HE materials have been undertaken [19]. However, a major challenge is the integration of non-cast energetic materials such as RDX with the SLS environment as safety is a major concern. These explosive particles do not necessarily melt and sinter due to energy input but may react violently. Therefore, a formulation process for high explosives and polymer binder solutions compatible with the SLS as an AM approach is required. It is also reported that individually coating each particle decreases sensitivity and submicron explosive particles organized into dermal safe clusters that maintain current infrastructure drastically increase weapon lethality, safety and performance against hard targets [20]. In order to achieve printable formulations of EMs via SLS, it is necessary to study the rheology of the formulations as well as the processing required. It is also paramount to comprehend the processes for a safer SLS of EMs.

1.3 Hypothesis

Individually coating energetic material particles with a binder allows for fabrication of energetic material compositions through selective laser sintering.

1.4 Aim

The aim of this study is to find a functional formulation process compatible with SLS of energetic materials.

1.5 Objectives

- To investigate and evaluate the coating processes that can be used with SLS to bind inert RDX simulant particles.
- To study the interaction of chemistry, particle geometry, examine the coating effectiveness and manipulate the material particle sizes at micro to mesoscale through formulations and AM.
- To evaluate some encapsulation/coating methods to prepare coated particles of simulant RDX as mock RDX and uses some characterisation techniques from literature. The simulant RDX used is comparable to those available in literature but the mock RDX prepared has not been documented elsewhere.

There are critical elements to consider during the formulation processes such as:

- Which binder is suitable (Polymer, wax, melt-cast HE)
- Chemistry and rheology is important
- Material strength (extreme requirements for warheads)
- Temperature capability
- Suitable type of laser and wavelength
- Maximize EM mass
- Minimize polymer binder/matrix (suitable material ratios)
- Minimize print voids.

1.6 Benefit

- Understanding the science behind coating formulations of high explosives and challenges that come with manufacturing of energetic materials additively may enable safe SLS of energetic materials to further improve research towards development of future munitions.
- The attempt to overcome these challenges is by developing process methods concentrating at the critical physico-chemical properties through formulations of mock RDX.

1.7 Scope and limitations

- Due to delineations such as safety and practicality during the investigation, the laboratory compositions prepared were inert.
- Only a pre-placed SLS method was used for binding purposes.
- Furthermore, no stability and sensitivity tests were conducted.

1.8 Brief Chapter Overviews

The dissertation begins with introduction to the research topic in Chapter 1. Chapter 1 includes the research hypothesis, aim, detailed objectives and ends with scope and limitations. It is followed by Chapter 2 which outlines the literature and theory regarding explosives and additive manufacturing. Chemical analysis techniques necessary for the investigation are also briefly highlighted. Chapter 3 outlines the experimental methodology. Characterisation of raw materials and compositions formulated is presented in Chapter 4. Results and discussions of the SLS trial tests are given in Chapter 5. Chapter 6 details conclusions and recommendations. Finally, Chapter 7 lists the references. Appendices A and B follow Chapter 7.

2 Literature Review

2.1 Energetic materials

Energetic materials are a class of material that can release chemical energy stored in their molecular structure. Upon external stimulations, such as heat, shock, or electrical current. These materials will emit energy in a short time. Based on their applications, energetic materials can be classified as explosives, propellants, and pyrotechnics.

The science of energetic materials is dedicated to developing means to predict performance and safety characteristics with high fidelity [10]. Explosives comprise primary and secondary explosives. The difference between these two categories of energetic materials is the sensitivity, initiation and performance. Primary explosives (i.e Lead azide and lead styphnate) are extremely sensitive and detonate easily by heat, spark, friction and mechanical shock [30]. While secondary explosives (i.e TNT and RDX) are relatively insensitive to heat, spark and shock and usually require initiation or detonation by a shockwave from a primary explosive. Both categories are refers to as high explosives due to their ability to release self-sustained high pressure and energy at detonation.

Explosives are expected to release large energy and expand greatly in volume to generate force in the time scale of μs. To achieve high power output, it is necessary to propagate reaction rapidly through the whole material, known as detonate. Detonation, deflagration, and regular fuel combustion are different phenomena distinguished by their rate-determining-step and propagation rate. For regular fuel combustion, the reaction rate is limited by diffusion of reactive species (mass transfer), which is relatively slow, leading to low propagation rate. In the case of deflagration, the oxidizer and fuel are premixed, therefore the diffusion of reactive species is no longer the rate-determining-step. Instead, the propagation of reaction zoom is controlled by heat transfer, resulting in its faster rate than regular fuel combustion. When energetic material detonates, the shockwave propagates through the material. At the wave front the material is highly compressed, leading to the temperature rise, which triggers exothermic chemical reactions and creates a chemical reaction zoom after the wave front. The exothermic reactions increase the temperature and pressure to the point higher than the condition before the passage of shock wave, which provide energy to sustain the propagation of shock wave.

Therefore detonation is in the speed of shock wave, which is supersonic, in contrast to the cases of deflagration and regular fuel combustion, which are subsonic. Several parameters can be used to characterize explosives, as described below.

i) Sensitivity: This represents how easily the explosives can be set off by external stimulus, such as impact, friction, shock, spark, and heat. Based on their sensitivity, explosives can be categorized into primary and secondary explosives. Primary explosives are highly sensitive and easy to undergo the deflagration-to-detonation transition (DDT). On the other hand, secondary explosives, or high explosives are less sensitive, but usually more powerful. A common way to take advantage of both explosives is to place a small amount of primary explosive adjacent to a large amount of secondary explosive, or so called explosive trains. The fast DDT of primary explosive helps to amplify the initial non-explosive impulse to shockwave, which then detonates secondary explosive.

ii) Heat of explosion (Q): This represents the amount of heat released from the decomposition of explosive during explosion. This quantity can be well approximated as the difference of the heat of formation of combustion products and explosive itself. Large heat of formation is preferred for explosives because it leads to higher explosive power, which is defined as the product of heat of formation and the volume of gas product.

iii) Detonation velocity (D): This quantity represents how fast the detonation wave propagates and therefore controls the rate of energy release of explosives. The value of detonation velocity increases with the density of packing of explosives in the column and is positively correlated with the detonation pressure. For most applications, such as rock cleaving and grenades, it is desirable for explosives to reach its peak pressure quickly to maximize the shattering power, and high velocity of detonation is necessary. The shattering power can be quantified by brisance, which is defined as the product of the loading density, the detonation velocity, and the specific energy (the maximum pressure through explosion multiplies volume of detonation gases) [30-31].

There are many factors that determine the practicality of explosives. For the secondary explosives, besides the performance requirements (high detonation velocity and large heat of explosion), it is very important to have low sensitivity and long term stability, which make it easier to store and handle these explosives in large amounts. The production cost is another important issue to determine [31].

2.2 Secondary high explosives

Secondary explosives also referred as high explosives are defined as an explosive substance or mixture which invariably detonates when initiated, irrespective of the ambient condition or confinement (i.e. in the open). They are compounds when initiated by shock, the reaction within the

product is supersonic, and has a high brisance. These explosives are relatively insensitive, in comparison to primary explosives and are insensitive to shock, friction, or heat. They are, however cap or booster sensitive [33], as illustrated by Figure 3.

RDX (structural molecule shown in Figure 5) is one of the powerful secondary high explosives. It is also known as Hexogen, Cyclonite and cyclotrimethylenetrinnitramine, a white crystalline solid with a melting temperature of 204 °C with molecular weight 222.1 $g.mol^{-1}$. It attained military importance during World War II since it is more chemically and thermally stable and has a lower sensitiveness and great explosive power. Pure RDX is very sensitive to initiation by impact and friction and is desensitised by coating the crystals with wax, oils or grease. Insensitive explosive compositions containing RDX can be achieved by embedding the RDX crystals in a polymeric matrix. This type of composition is known as a polymer bonded explosive (PBX) and is less sensitive to accidental initiation [32]. It is difficult to dissolve in organic liquids but can be recrystallized from acetone. Because of its high melting point, it is difficult to melt cast or melt-cure by energy or heat. However, it can be mixed with TNT or a binder, which has a low melting temperature.

RDX is of particular interest for this study has 2 different polymorphs defining the crystal structure. Polymorphism within energetic materials (both primary and secondary) is a main cause of concern for sensitivity. Numerous studies on the polymorphism of RDX show that there are five phases: α, β, γ, δ, and ε [34]. Of these five forms, only α-RDX and β-RDX exist at room temperature and ambient pressure, α-RDX (molecular conformation of −NO2 groups: axial–axial–equatorial) and β-RDX (molecular conformation of −NO2 groups: axial–axial–axial) as can be seen in. Hultgren [34] first described α-RDX crystals as orthorhombic. Torres [35] described the β-polymorph as structures resembling islands as well as scattered particles. Goldberg and Swift [36] described both α-/β-RDX polymorphs (shown in Figure 4) as assuming a variety of different morphologies, and concluded that α-RDX is the most stable crystal form at room temperature and ambient pressure.

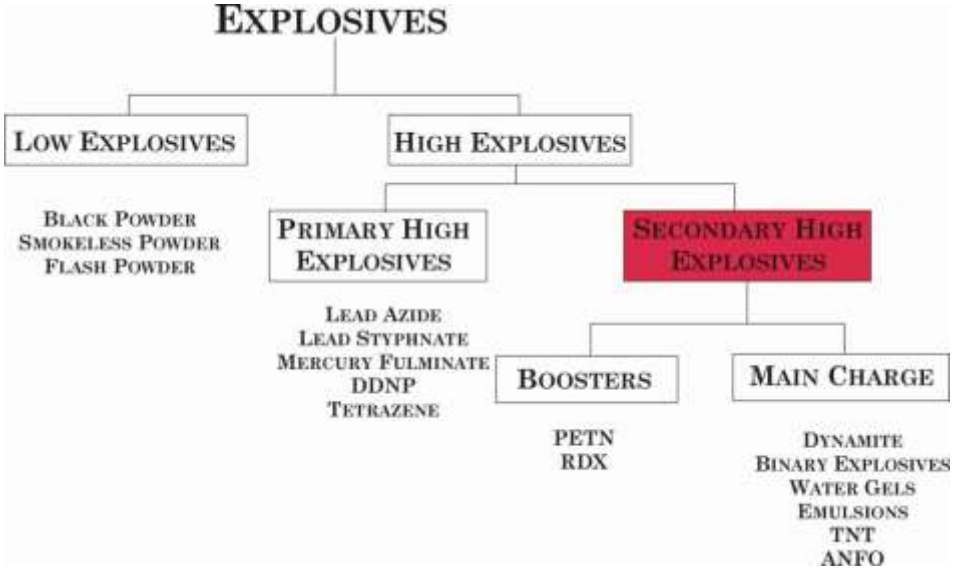

Figure 3: Classification of explosives [33].

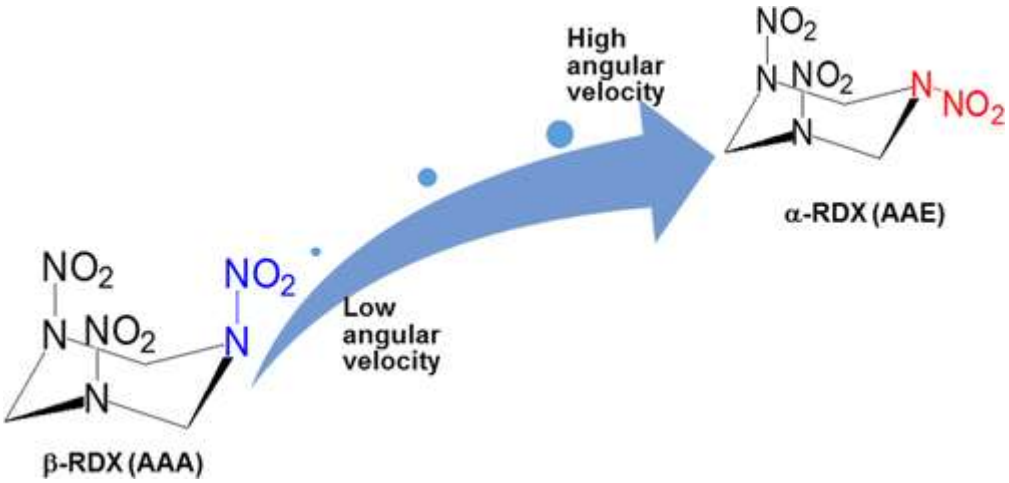

Figure 4: RDX structural polymorphs stable at room ambient conditions [36].

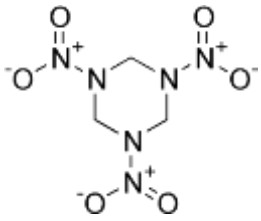

Figure 5: RDX structural molecule [37].

As reported by Akhavan [32], there are also two types of of RDX, type A and B. Type A RDX has no impurities, while Type B contains impurity level of 8-12%. The RDX explosive material of

particular interest is a production grade (A), Type A, as a fine crystalline material about 20-80 and 2-10 microns diameter which have been utilised in propellants and warhead formulations. Although the very-fine (micron range) crystals of RDX explosives are less sensitive to friction and more uniform than larger crystals of the nitro-amines, such very-fine crystals have a very large active surface which is negatively charged, resulting in a serious electrostatic safety problem when the nitro-amine explosives are handled in a dry state. Thus, for example, accidental explosions in plant production can occur during handling of the very-fine crystal nitro-amine explosives in the raw, neat state [37-38]. Thus, there is a need for safer processing of very fine crystals of nitro-amine, especially when it comes to heat or energy produced during manufacturing.

Some explosive mixtures require the use of binders to for safety during processing and handling. Binders are compositions that hold together a charge of finely divided particles and increase the mechanical strength of the resulting propellant grain. The addition of inert or energetic binders has reduced the sensitivity of PBXs while improving the processability and mechanical properties [32]. These are usually functionally terminated prepolymers such as hydroxy-terminated polybutadiene (HTPB), carboxyl-terminated polybutadiene (CTPB), Polycaprolactoen,resins, plastics, or asphaltics used dry or in solution. The enthalpy of formation (ΔH_f) should be more positive and the binder must have suitable structure, which on combustion produces low molecular weight gases, thereby leading to high specific impulse [40]. The incorporation of binders on energetic particles is usually through coating or binding processes.

2.3 Particle size, morphology and voids

Thermal stability and sensitivity of RDX to shock is dependent on manufacturing methods and crystal size. However, It is not the particle size by itself that influences the sensitivity of the explosive material but the particle size relative to the size of the voids. It is reported that large structures of RDX are without voids, therefore not allowing hot spots for a shock stimulus to generate the conditions needed to start and sustain a chemical reaction [41]. And although there is some heat generated due to collisions of the particles, there is negligible heat generation on a microscopic level which results to insignificant increase in temperature [42]. In theory, the critical diameter of a “hot spot” is between 0.1 and 10 μm. Shock sensitivity will decrease with the decrease of void size as the void size approaches the width of the shock front about 4 micrometres and electrostatic discharge (ESD) values are greatly influenced by the particle size [41]. It is worth noting that the desensitization may interfere with the hot spots. The formation of localized hot spots has been generally attributed to the presence of pores, which facilitate the inadvertent initiation and a consequent detonation of explosives. [43].

Conversely, reports show that the impact and friction sensitivity of EMs is determined by the degree of particles fineness, moisture content and temperature. The sensitivity increases with a reduction in particle size and increase in temperature. It is therefore important to understand the hot spot theory of explosives before manipulating the crystal morphology. Hot spots can be generated by; (1) friction, whereby the interstices offer no resistance when a shockwave dislocates them and the presence of grit crystals rubbing together increase the sensitivity of the explosive material. Should one look at the crystals of an explosive when it detonates, one would see the crystals jostle together due to the shockwave passing through and where they touch are the areas of friction called “hot spots”; (2) Compression of gas bubbles, whereby the energy from the shock wave is converted to heat by adiabatic compression of small, trapped bubbles of gas in voids; and cracking of the crystalline explosive materials [44]. Therefore, by at least reducing the “hot spots”, a substantial desensitization of explosives can be achieved but at the expense of performance. On the contrary, some studies conducted [42-46] have proven the reduction in crystal size as a viable option to desensitization of nitro-amine high explosives as it should lead to a lowered sensitivity.

Sensitivity of a HEM to incident energy is associated with chemical structure, physical properties (crystal size, shape, defects) and formulation characteristics (binder material /processing). Some effects of size reduction include; smaller size of crystal defects, smaller size of inter-crystal voids, improved mechanical properties and enhanced resistance to plastic deformation. Due to a larger number of heterogeneities with smaller dimensions a more homogeneous distribution of incident energy and shock spreading is greatly improved [42]. It is also reported that ultrafine RDX less than 5 µm, round and rod shape, is more sensitive to impact and less sensitive to friction compared to the production grade (60-80 µm) [27]. They are also more sensitive to spark compared to coarse particles, unless the sample is of different morphology.

The narrower distribution means a smaller packing fraction of particles which will increase porosity of prints. Since the highest density of particles is in the lower micron range, agglomeration is also a factor which must be considered throughout manufacturing due to the small size of the particles. The desired particle shape is formed relative to the solvent mixture, temperature at mixing, and agitation. This study makes use of the results on the literature during characterisation to compare the simulant particle size with the RDX production grade. Therefore there are many factors to consider before selecting a particle size [47]. A suggestion is using particles in the micron-sized range (less agglomeration than nanoparticles) with a broader size distribution for increased packing fraction so that less binder must be added for full densification. It Is been reported, the particle size in the range of 20-100 µm is preferred for the SLS of polymer based particles [16-18].

2.4 Binding processes

2.4.1 Polymer Binding

Due to vulnerability of RDX, binders are commonly employed in desensitization in polymer bonded explosives (PBX). Previous studies have focused on the crystallisation of RDX and its simulant and co-crystallisation with polymers to produce desired forms of crystals [39,45,48-52]. Pant, A and Amiya, K.N (2009) precipitated RDX from acetone solution by reducing the solvent power using an anti-solvent or an aqueous anti-solvent containing water [27]. Other authors used the Precision Particle Fabrication technology to produce polymer-coated high explosive particle spheres [24]. Studies have been conducted using simulant explosive materials to examine coating effectiveness and density [44]. Some common military explosives are compared to simulants L-tartaric acid and sucrose. Konek [53] utilised L-tartaric acid as a simulant for RDX. Nampi (2011) [54] studied the binding of PVA on Alumina as a energetic material simulant.

It is reported that various plastic bonded explosives (PBXs) contain about 5-10 wt% of binder composed of a polymer, a plasticizer, and a stabilizer. The glass transition temperature (T_g) determines, to some degree, if the binder will reduce or increase the sensitivity of the PBX to impact [55]. A soft binder reduces the impact sensitivity. However, too soft a binder compromises the mechanical strength below that desirable for dimensional stability [44]. Because RDX is not the most sensitive explosive and it is not necessarily a requirement to use a more rubbery binder and softer to cushion it from accidental stimuli during processing, such as the friction and shock [56]. For this material, it is desirable to use a polymeric binder with a T_g below the temperature (<zero degrees Celsius) of use for reliable binding of the simulant crystals and desensitization. The binder also needs strength to achieve the desired mechanical behaviour of the polymer coated explosive during the AM process. To achieve this, polymeric material is used to facilitate the sintering and binding of RDX particles through AM processes.

Many research reports indicate that when nitro-amine explosives are coated with some inert materials such as polymers, wax, graphite and stearic acid, the mechanical sensitivity could be reduced [22,60-63]. For examples, Wang, J [57] prepared a 95% HMX, 4% Viton and 1% Graphene Oxide and were able to demonstrate from their DSC results that the thermal stability is enhanced. Manning [59] coated high explosives with graphite and the outcomes showed that the impact sensitivity of the coated material was decreased by 40% and the coated shell increased the ignition delay.

Studies proved [38] that by thinly coating the nitro-amine crystals with, e.g. about 0.05 to 0.2% by weight polyvinyl pyrrolidone (PVP) as a complexing agent, the electrostatic handling problem is

greatly diminished. Yang [58] fabricated RDX, HMX and CL-20 with 2.9 to 3 wt.% melamine-formaldehyde resins to reduce the sensitivity and found that the thermal and impact sensitivity was reduced with increased polymorphic phase transition and thermal decomposition temperatures.

Polymer coating on RDX has been undertaken before through a slurry technique, whereby RDX was coated with dinitrotoluene (DNT), polyvinyl acetate (PVAc) and stearic acid (SA) as a surfactant with a mass percentage of RDX:DNT:PVAc:SA is 94.5:3:2:0.5 [60]. Moreover, there is still a need for more binders test for better coating. da Costa Mattos [22,65] undertook studies on the characterisation of polymer- coated RDX using Viton as a binder.

2.4.2 Binding by melt-cast explosives

RDX has been mixed with a melt-cast explosive, TNT, to lower the its melting point, thermal ignition temp 260° C, to increase chemical stability and decrease sensitivity [32]. In order to decrease the mechanical sensitivity of RDX while maintaining its explosive performance, Lu and Zhou prepared a composite explosive through coating RDX with TNT and a plasticizer as an insensitive method of coating sensitive high explosive RDX with a less sensitive explosive TNT was studied. The authors coated RDX with a little TNT and energetic plasticizer by melting, dispersion and cooling crystallization to RDX surface in water, a kind of double-deck composite explosive with low mechanical sensitivity, in which inside layer is RDX and outside layer is TNT, was prepared by adding TNT 3%-10%, energetic plasticizer [66-67].

2.5 Mock high explosives

Tartaric acid and sucrose have been used as simulants for RDX for analytical and characterisation studies [53]. Polymer coating of explosive mock powder has been studied, characterised and tested [21,23,55] for safety performance. Hunt [22] examined the method to develop a PBX whereby a synthetic polymer (5-10% by weight) matrix was used to bind the explosive simulant and explosive materials through precision coating process.

2.6 Coating methods

Many microencapsulation techniques are available such as spray drying, fluidised-bed coating, coacervation, electrospraying and supercritical carbon dioxide assisted Microencapsulation, slurry processes and emulsions [64]. Polymer coating on RDX has been undertaken before through a slurry technique [63-64]. RDX was coated with dinitrotoluene (DNT), polyvinyl acetate (PVAc) and stearic acid (SA) as a surfactant with a mass percentage of RDX:DNT:PVAc:SA is 94.5:3:2:0.5 [60]. Other researchers used the Precision Particle Fabrication technology to produce polymer-coated high

explosive particle spheres [24]. Elizabeth da Costa Mattos et al, (2008) undertook studies on the characterisation of polymer- coated RDX using Viton as a binder [22,65]. Studies have been conducted using simulant explosive materials to examine the polymer coating effectiveness and density prepared through a slurry process [52].

Polymer coated explosive mocks have been studied, characterised and tested for safety performance [36,46,55]. Some common military explosives are compared to simulants L-tartaric acid and sucrose for analytical studies. Konek [53] utilised L-tartaric acid as a simulant for RDX. Hunt [22] examined a method to develop a PBX whereby a synthetic polymer (5-10% by weight) matrix was used to bind the explosive simulant and explosive materials through precision coating process. Nampi [54] studied the binding of PVA on Alumina as an energetic material mock. The solvent evaporation method to produce polymer encapsulated materials has been studied extensively in the pharmaceutical research due to the compatibility and shelf-life of the polymers used [65].

Stepanov [66] manufactured RDX nanoparticles with a narrow particle size distribution of 110-220 nm using the rapid expansion supercritical solution process. Lee [71-72] prepared micronized RDX using the supercritical anti-solvent (SAS) process to examine the influence of different solvents on the morphology, particle size, and particle size distribution (PSD). The slurry process was used to formulate PBXs (PBX 9501 and PBX 9502), whereby the crystalline explosive was slurried in water and binder dissolved in an organic solvent, which is not miscible in water. After the binder solution was added, the mixture comprised solid plus two liquid phases was turbulently mixed. The second solvent phase removed either by distillation or addition of water to achieve a single liquid phase system in which small beads of PBX are insoluble. The crystalline explosive, covered by the binder in this manner, is called moulding powder. The moulding powder filtered off, dried, and pressed [55].

To improve the safety of RDX (hexogen), Wei [62] made use of an energetic polymer (HP-1) to coat RDX with 2,4,6-trinitrotoluene (TNT) by combining the solvent – nonsolvent and the aqueous suspension-melting method. The RDX was slurred in water at 85°C and the solution of TNT plus plasticizer was added onto the slurry under vigorous stirring and cooled to 50 °C evapourated at 40°C.

The coating process of the crystalline explosives, such as RDX and HMX has been reported. The process is reported to have been through the use of the slurry method whereby the explosive material is slurred in water (aqueous phase) and the polymer is dissolved in an organic solvent with low boiling point, not miscible with water, that is added during the process. This process is carried out under strong stirring (500 – 700 rpm) [57,73]. The solvent is removed by distillation under continuous

stirring, and the polymer precipitates on the surface of the crystals of the explosive at the end of the solvent elimination. The authors reported that after the coating process of the granular product is formed, it can be used in pressed explosive charges with high-energetic content [22,73], and AM process.

The solvent evaporation method to produce polymer encapsulated materials and energetic materials has been studied extensively due to the compatibility and shelf-life of the polymers and binder used [65]. The coating process of particles was done through oil-in-water (O/W) and oil-in-water-in-water (O/W/W) emulsions. In the solvent evaporation the polymer was dissolved in a suitable water immiscible solvent, and the material or simulant to be fabricated is dispersed or dissolved in this polymeric solution. The resultant solution or dispersion was then emulsified in an aqueous continuous phase to form discrete droplets. In order for the microspheres to form, the organic solvent must first diffuse into the aqueous phase and then evaporate at the water/ air interface. As solvent evaporation occurs, the microspheres harden and free flowing microspheres can be obtained after suitable filtration and drying [47,69].

2.7 Laser

The term "laser" is an acronym for light amplification by stimulated emission of radiation. It is generally a device that emits light via a process of optical amplification based on the stimulated emission of electromagnetic radiation. The laser is seen as playing a pivotal role in the growth of AM systems and metal AM, in particular recently. It is at the “heart” of metal AM technology, and its developments in terms of power, efficiency, beam quality, and reliability parallel the growth and application of metal AM systems globally [4].

The laser AM approaches involve “powder or wire-fed” or laser metal deposition and “powder bed” or selective laser melting. In general it can be said that these technologies have significantly affected the manufacture of new components and maintenance, repair, and overhaul of small and large components in the aerospace, defence, power generation, mining, and general manufacturing industries globally and will continue to do so in the future. In the case of polymer powder processing, the CO_2 laser is the laser of choice because of the high polymer absorptivity at the CO_2 laser wavelength. Similarly, for the processing of photo polymers, blue diode lasers have replaced traditional ultraviolet lamps [4,74].

Laser-based AM processes concentrate the heat to a relatively small localized area of the part based on the laser spot size. Hence high precision is achieved, with good metallurgical bonding between layers and relatively low distortion because of the low heat input. The manufacturing process itself is

very complex, with many variables, such as laser power, scan speed, hatch spacing (center-to-center distance between single tracks), powder particle size morphology, distribution, layer thickness, and scan strategy, all playing important roles in producing fully dense with minimal internal stress [4].

In the case of polymers or photopolymers, the absorbed laser light polymerizes or hardens the area of the polymer that it irradiates, producing a solid part. When a laser beam impinges on the surface of a material, either a solid, powder, or liquid-some light is reflected, some is absorbed, and some may be transmitted, depending on the optical properties of the work piece. The fraction of the laser beam that is absorbed by the surface of a material in the case of metals is transformed into heat through electron-phonon interaction, and this heat raises the temperature of the surface to achieve the required melting state of the material for AM. Laser output power, spatial distribution, time dependence (pulsed or continuous), beam diameter, and beam divergence affect how well the beam can be controlled in terms of the rate at which energy can be delivered to the material and how this energy is distributed spatially. Wavelength is a key factor in determining the laser most suitable for a particular process. The coupling of energy into the material will be zero, and consequently no heating or change of state will occur unless a wavelength at which there is some absorption is selected [70].

It is reported on some studies that the condition of the explosive surface, such as particle size, density, and reflectivity, affects the laser sensitivity of the material [71]. On these studies, the RDX failed to initiate at the energy level of 5J, 15J with energy density of approximately1500 J/cm^2 from a CO_2 and He-Ne IR laser beams. If the RDX materials exposed to the laser beam are highly confined, the pressure from reaction products that facilitates the propagation would be sustained and self-propagation reaction may occur. Trzcinski and Ming-Wei [27,76] utilised a long-wavelength infrared (LWIR) to irradiate the RDX crystals. The authors showed that the weakly absorbed wavelengths create hot spots than strongly absorbed wavelengths. They substantiated their findings that when pulses of LWIR are long-duration and low intensity. But if the LWIR were intense and long-duration, then the RDX crystal surfaces would be much hotter in the strongly absorbed regime, and hence resulting into ignition. Hence, a binder is required to facilitated the bonding process.

2.8 Thermochemistry of explosives

The α and β forms of RDX are said to exist at a metastable state at ambient conditions. However, if they are activated by stimuli, they start reacting exothermically. During that process, the energy is absorbed to a minimum energy required to form hotspots. If the energy generated by the hotspots is less than the activation energy, no reaction will take place. Thus the hotspots will gradually die out [32], as illustrated in Figure 6.

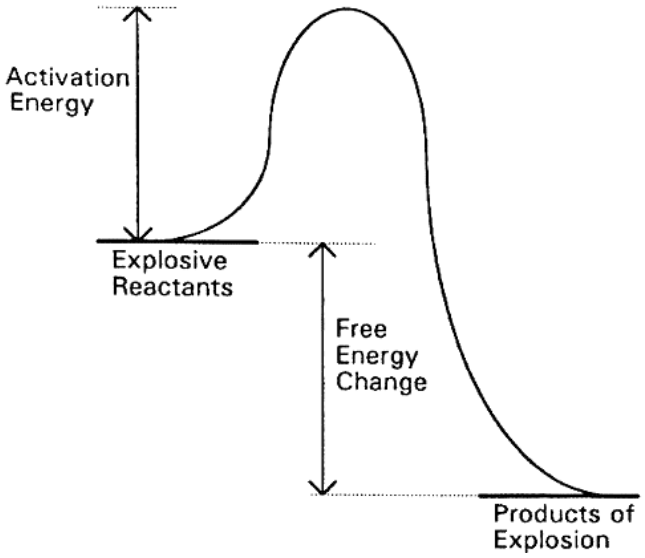

Figure 6: Schematic diagram of the activation reaction profile for explosives [32].

2.9 Characterisation techniques

Fourier transform-IR spectroscopy (FT-IR) in transmission and photoacoustic detection (PAS) techniques have been used for the characterization of polymeric coating of RDX) and HMX using a fluoro -elastomer (Viton). The FT-IR is used to determine the polymer content in the coated particles [9,40]. The Atomic force microscopy (AFM), scanning electron microscopy (SEM), X-ray diffraction (XRD), X-ray photoelectron spectroscopy (XPS), and differential scanning calorimetry (DSC) were employed to characterize the morphology, composition, and thermal decomposition of samples polymer bonded explosives [8-9, 27,30].

2.9.1 Particle size distribution

Particle size may affect both the formulation and the manufacturing process (AM). It is therefore important to understand the size distribution suitable for SLS application. The energy can be absorbed or scattered by the particles, depending on the particle morphology, size and concentration. Penttilä and Lumme [73] studied the effect of particle shape on the efficiency of light scattering. They showed that the projected area of the particle has a key role in scattering, but the effect is different for different sized particles and changes systematically and can be different from the solution of closely packed material from the same particles.The light scattering of a single particle is mostly affected by three key factors: the size of the scatterer (compared to the wavelength), its shape and its refractive index. It is emphasized that the laser light scattering is greatly influenced by smaller, closely packed and irregular shaped larger particles. Therefore, to avoid light scattering the wavelength used should be lesser than the particle diameter and particles more loose and regular. Some samples there comprised bigger particles formed of smaller ones, and some samples had smaller and agglomerated particles may cause slight scattering [78-79].

2.9.2 Morphology and shape

Scanning Electron Microscopes (SEM) scan a sample with a focused electron beam and deliver images with information about the samples' topography and composition.

The scanning electron microscope (SEM) uses a focused beam of high-energy electrons to generate a variety of signals at the surface of solid specimens. The signals that derive from electron-sample interactions reveal information about the sample including external morphology (texture), chemical composition, and crystalline structure and orientation of materials making up the sample. In most applications, data are collected over a selected area of the surface of the sample, and a 2-dimensional image is generated that displays spatial variations in these properties. Authors have used this technique to analyse and measure both coated and uncoated particles and crystals [22,42,80-81].

2.9.3 Organic and inorganic molecule characterisation

Fourier transform infrared spectroscopy (FTIR) is a rapid, non-destructive, time saving method that can detect a range of functional groups and is sensitive to changes in molecular structure. FTIR provide information on the basis of chemical composition and physical state of the whole sample [78]. Fourier-transform Raman spectrometry is a powerful tool for the investigation of compound characteristics at a molecular level and providing complementary information to that obtained by Fourier transform infrared micro-spectroscopy. In addition the sensitivity and accuracy of FTIR detectors along with wide variety of software algorithms have dramatically increased the practical use of infrared for quantitative analysis [83-84].

FTIR analysis identifies chemical bond functional groups by their characteristic absorption of infrared radiation in vibrational modes. It may be used in transmission mode. In attenuated total reflectance (ATR) mode, the detection depth is generally 1-2 μm deep, but can be much less or a bit more dependent upon the material. Black, highly absorbing materials tend to have smaller sampling depths and sometimes provide too weak a signal as a result. FTIR is especially capable of identifying the chemical bonds of organic materials. Detects and identifies organic contaminants or additives. Determines bonds undergoing degradation reactions or changing with processing. Identifies water and carbonate, phosphate, sulfate, nitrate, nitrite, and ammonium ions, silica, silicones and other inorganic chemicals. Detection limits vary greatly, but are sometimes <1013 bonds/cm^3 or sometimes sub monolayer

Useful in characterizing solids, liquids, or gases wavenumbers (cm^{-1}), the inverse of wavelengths (cm), are plotted for convenience. Structural features such as the backbone or functional groups of a molecule can be identified by characteristic absorptions produced in the spectra (Coates, 2000). The

fingerprint region in the range between 400 – 1500 cm^{-1} is used to identify unknown samples while absorption bands between 1500 – 4000 cm^{-1} are used to determine functional groups within a sample.

2.9.4 Thermal analysis

Thermal analysis includes a broad range of techniques. In fact, any measurement where the temperature is controlled and recorded with respect to time may loosely be defined as thermal analysis. Differential scanning calorimetry DSC is the most popular form of thermal analysis (Figure 7) and has been routinely applied in the pharmaceutical sciences since the 1970s. DSC is used to measure the heat flow in and out of both a sample and reference crucible during a controlled temperature programme. The sample crucible usually contains the API or material under study and the reference crucible is either left empty or is loaded with an inert reference material relevant to the sample under investigation. The crucibles are usually aluminium pans and contain 1 to 10mg of sample. Two general types of DSC are available that measure heat flow in slightly different ways; power compensated and heat flux DSC. Both types of DSC apply the temperature programme via heaters using a furnace type arrangement. The temperature programme is commonly linear heating at a rate of 10°C/min. Heat flux DSC (Figure 7 (b)) comprises a single heating block with thermocouples used to monitor the temperatures of both the sample and reference crucibles. The temperature differential between the sample and reference is used to determine the heat flow associated with transitions and reactions within the sample crucible as a function of the temperature programme. Power compensated DSC places the reference and sample crucibles in two separate furnaces. The temperature of the sample and reference is monitored again by thermocouples and heat flow is adjusted between the sample and reference furnaces by use of separate heaters to maintain the same temperature in both crucibles. In such a way the difference in heat flow or power between the two crucibles is compensated and a direct measure of the heat flow from the sample as a function of the programmed temperature is recorded. There are a number of reviews and books that describe the theoretical and experimental aspects of DSC. DSC has been used to analyse thermal attributes on different materials, including explosives [85-86].

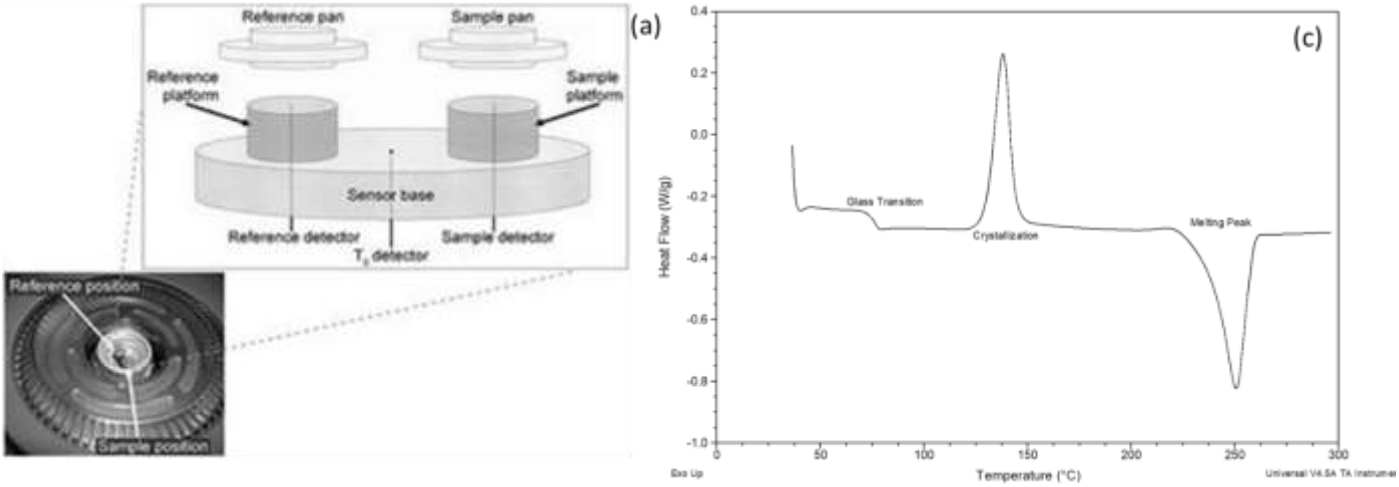

Figure 7: heat-flux configuration; (a) Classical apparatus (b) Typical DSC curve.

2.9.5 Compound/molecule composition

X-ray diffraction (XRD) is a non-destructive technique used to characterise the crystallographic structure, grain size, and orientation is polycrystalline materials. It is also used to identify structures of unknown substances, as well as phase analysis [83]. Other applications of XRD analysis include determination of phase transitions in a given substance, semi-qunatitative determination of phases present in a sample, measurement of crystallite size particularly in nano materials, analysis of stress and crystal structure analysis by Reitveld refinement. It uses Bragg's Law is:

$$n\lambda = 2d \sin\theta, \quad (1)$$

Where λ is the wavelength of x-rays, d is the interplanar spacing θ is the x-ray angle n is an integer. The diffraction process occurs when the Bragg's law (condition) is satisfied. It is expressed as in Figure 8:

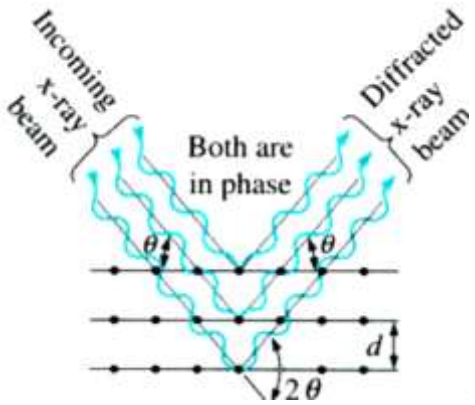

Figure 8: X-ray diffraction principle [84].

2.9.6 Particle packing theory

The particle packing arrangement is very important for the AM processes for energetic materials [16-18]. The packing arrangement determines whether the product is densified or not (with or without voids). The packing density is theoretically defined as:

$$\varphi = Vs/Vt = V_s/(V_s + V_v) = 1 - \varepsilon \quad (2)$$

Where, φ is the packing density, Vs and Vv are the volume of solids and voids respectively. Vt is the total volume and ε is the porosity.

2.9.6.1 Close-packing of equal spheres (dense packing)

Two simple arrangements within the close-packed family correspond to regular lattices. One is called cubic close packing (or face centred cubic, "FCC")—where the layers are alternated in the ABCABC... sequence. The other is called hexagonal close packing ("HCP")—where the layers are alternated in the ABAB... sequence. But many layer stacking sequences are possible (ABAC, ABCBA, ABCBAC, etc.), and still generate a close-packed structure. In all of these arrangements each sphere is surrounded by 12 other spheres, and the average density is 64%

$$\frac{\pi}{3\sqrt{2}} \simeq 0.74048. \quad (3)$$

In geometry, close-packing of equal spheres is a dense arrangement of congruent spheres in an infinite, regular arrangement (or lattice). Carl Friedrich Gauss proved that the highest average density, that is, the greatest fraction of space occupied by spheres that can be achieved by a lattice packing is 74% [85].

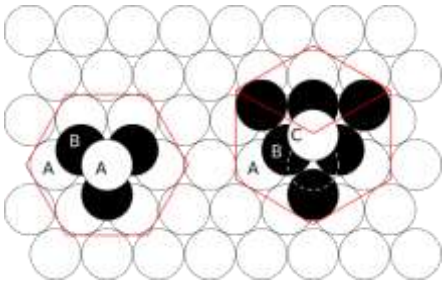

Figure 9: Illustration of the close-packing of equal spheres.

2.9.6.2 Random packing

When spheres are randomly added to a container and then compressed, they will generally form what is known as an "irregular" or "jammed" packing configuration when they can be compressed no more. This irregular packing will generally have a density of about 64%. Recent research predicts analytically that it cannot exceed a density limit of 63.4% [86]. This situation is unlike the case of one or two dimensions, where compressing a collection of 1-dimensional or 2-dimensional spheres (that is, line segments or circles) will yield a regular packing.

$$\frac{\pi}{3\sqrt{3}} \approx 0.6046 \qquad (4)$$

Many problems in the chemical and physical sciences can be related to packing problems where more than one size of sphere is available. Here there is a choice between separating the spheres into regions of close-packed equal spheres, or combining the multiple sizes of spheres into a compound or interstitial packing. When many sizes of spheres (or a distribution) are available, the problem quickly becomes intractable, but some studies of binary hard spheres (two sizes) are available.

When the second sphere is much smaller than the first, it is possible to arrange the large spheres in a close-packed arrangement, and then arrange the small spheres within the octahedral and tetrahedral gaps. The density of this interstitial packing depends sensitively on the radius ratio, but in the limit of extreme size ratios, the smaller spheres can fill the gaps with the same density as the larger spheres filled space [87].

2.9.6.3 Unequal sphere packing

When more than one size of sphere is available in the mixture or powder, combining the multiple sizes of spheres into a compound or interstitial packing can also increase density. When the second sphere is much smaller than the first, it is possible to arrange the large spheres in a close-packed arrangement, and then arrange the small spheres within the octahedral and tetrahedral gaps. The density of this interstitial packing depends sensitively on the radius ratio, but in the limit of extreme size ratios, the smaller spheres can fill the gaps with the same density as the larger spheres filled space [87]. Even if the large spheres are not in a close-packed arrangement, it is always of advantage to insert some smaller spheres of up to 0.29099 of the radius of the larger sphere [88]. The literature also reports that a way to create a denser sintered layer is to create a more dense bed prior to the sinter [52][89][90][91][92]. This means mixing different sizes or grades of particles and the particle sizes should be designed and mixed in proportion to better fill space in your sinter bed to maintain a heterogeneous packing state well and reduce voids. Research has shown that packing the coarser grains with smaller particles not only yields higher density powders but also decreases balling defects

in the finished printed product [89].

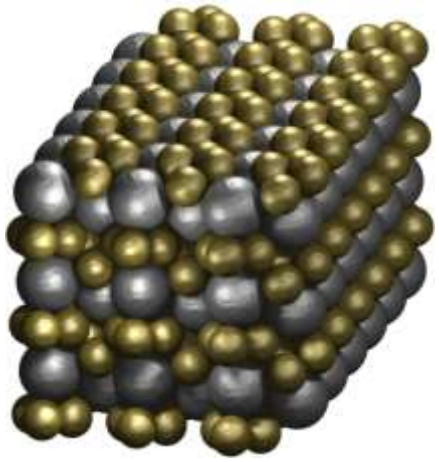

Figure 10: A dense packing of spheres with a radius ratio of 0.64799 and a density of 0.74786 [92].

2.10 Additive manufacturing of explosives

Gash [7] studied and developed the methodology for AM of formulated and characterised plastic-bonded explosives components, whereby the product consisted of 94% explosive crystal material by weight bonded together as an agglomerate by 6% plastic polymer. Previous studies and current PBXs involve coating the HMEs with plastic wax.

The most important powder property is depositability, which depends on the size and shape of the particles. Deposition can be performed with the powder in either a dry or wet state, but the acceptable particle sizes are different for each deposition process. Particles that are 20 microns and larger are preferably deposited in the dry state, while particles smaller than 5 microns can be deposited in either the dry or wet state [35]. Fine powders (~1 micron) tend to agglomerate due to van der Waal's forces and moisture effects [36], so mechanical spreading can be problematic. Fine powders can be deposited in a dry state, but only as a low volume percentage in a predominantly larger diameter powder formulation or as bound agglomerations of smaller particles [37]. Fine particles can instead be deposited as a slurry when the particle size is less than about 5 microns [35]. The spherical powders are preferred for dry deposition because they tend to flow better [2] and have low internal friction [37]. Faceted or anisotropic powders have much more frequent interparticle contact than spherical powders, and the increased internal friction lowers the spreadability of powders with these particle shapes, but may increase the packing ratio [37]. The particle size affects design parameters of both the printing process and the final part. Some parameters affected include sinterability, pore size, surface area, surface roughness, and minimum feature size. Fine powders have the potential advantages of increased sinterability, lower surface roughness, smaller minimum features, and thinner

layers [36]. Larger particles are easier to spread, have lower surface area per volume [38], and the larger pores facilitate fluid migration through the bed to aid in the production of more homogeneous parts [39]. Multimodal powder formulations containing a variety of particle diameters can offer the benefits of both small and large particle sizes. The large particles allow the powder mixture to be spread in a dry state, while the smaller particles fill the interstices between the large particles to increase the bed density [43] and offer the aforementioned smaller particle size benefits. The potential density increase can be particularly significant [20].

Powder bed fusion processes consist of thin layers of very fine powders, which are spread and closely packed on a platform. The powders in each layer are fused together with a laser beam or a binder. Subsequent layers of powders are rolled on top of previous layers and fused together until the final 3D part is built (as demonstrated in Figure 2, Section 1.1). The excess powder is then removed by a vacuum and if necessary, further processing and detailing such as coating, sintering or infiltration are carried out. Powder size distribution and packing, which determine the density of the printed part, are the most crucial factors to the efficacy of this method [14].

The laser can only be used for powders with a low melting/ sintering temperature, whereas a liquid binder should otherwise be used. Selective laser sintering (SLS) can be used for a variety of polymers, metals and alloy powders while selective laser melting (SLM) can only be used for certain metals such as steel and aluminium. Laser scanning in SLS does not fully melt the powders and the elevated local temperature on the surface of the grains results in fusion of the powders at the molecular level. On the other hand, the powders are fully melted and fused together after laser scanning in SLM, which results in superior mechanical properties [15]. The chemistry and rheology of the binder or the coated particles, size and shape of powder particles (coated particles), deposition speed, the interaction between the powder and binder, and post-processing techniques play an important role in 3DP [13,14]. The porosity of parts printed by binder deposition is generally higher compared to laser sintering or melting, which can print dense parts [14]. Laser power and speed of scanning are the main parameters affecting the sintering process [15].

3 Experimental

3.1 Materials

Figure 11 shows the structural molecule unit of the coating binders. Poly-ε-caprolactone (PCL) and 3,4,5-trimethoxybenzaldehyde (utilised as TNT simulant) with melting points of 60 ºC and 73-82 ºC, respectively, were explored as potential coating materials and binders. PCL is a biodegradable polymer used in pharmaceutical research (for particle encapsulation) for improved stability and shelf-life, solubility enhancement and controlled sensitivity. It has been used as an energetic polymer in pyrotechnic compositions. The 3,4,5-trimethoxybenzaldehyde obtained as a light yellow flake and it mimics TNT physical and chemical attributes (except for energetics). The molecular weight is 196.6 g/mol; the density is 1.40 g/cm^3; the melting is virtually the same as that for TNT and deflagration point is 337 ºC. The binders were obtained from Sigma Aldrich and used as received.

The selection of the simulants was informed by the extent to which they mimicked RDX with respect to its actual thermal and physical properties, including solubility in organic solvents but highly sparing solubility in water. Potassium bitartrate, purchased from Sigma, was chosen as the first RDX simulant. It has a melting point of 230 ºC, the molecular weight is 188.18 g/mol and it has a density of 1.05 g/cm^3, and it had the required solubility profile. Its unit molecule is shown in Figure 12(a). DL- Tartaric acid (DL-TTA), the second RDX simulant, has a molecular weight of 159.087 g/mol, density 1.79 g/cm3 (which is equivalent to that of RDX) and melting point of 206 ºC. The structural unit of DL-TTA is shown in Figure 12(b). Polyvinyl alcohol (PVA) was used as a stabiliser for the emulsification the formulations. The grade used had a molecular weight of 22000 g/mol and the degree of hydrolysis was 86–88%. Reagent grade dichloromethane (DCM), acetone, cyclohexanone and chloroform were also purchased from Sigma. All chemicals were used without further purification.

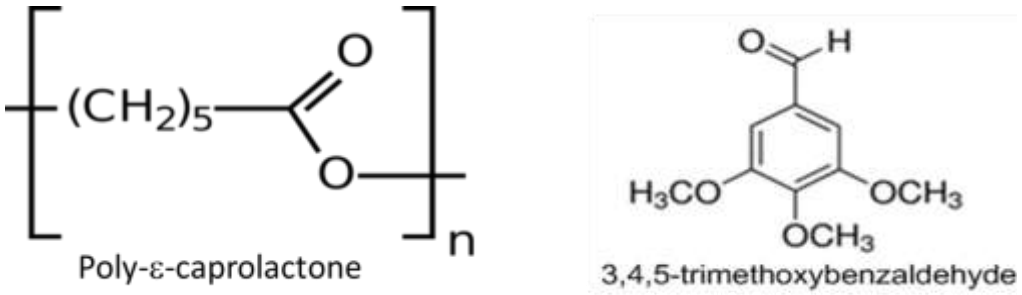

Figure 11: Structural unit of binders; polycaprolactone and TNT simulant (3,4,5-trimethoxybenzaldehyde) used.

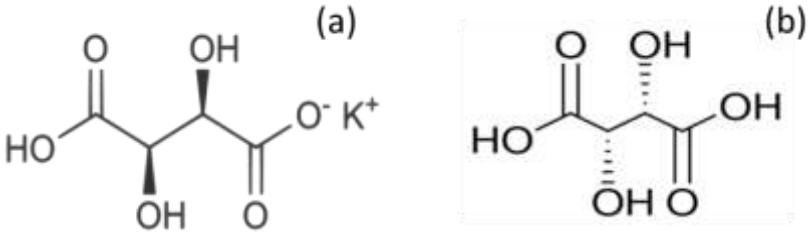

Figure 12: Structural unit of (a) Potassium bitartrate, and (b) dl-Tartaric acid enantiomer [93].

3.2 Methodology

Figure 13 shows a schematic diagram of the preparation mechanism through selected formulation methods towards a pre-placed SLS of mock RDX composites. From these formulation routes, the film and the coated particles were evaluated and characterised for coating effectiveness, particle morphology and size. The influence of these constraints was investigated on the SLS process, evaluating their effect towards fused or packed coated particles. The powder characteristics affect the sinterability, pore size, surface area, and surface roughness. The particle size affects design parameters of both the printing process and the final part. The most important powder property is depositability during SLS process, which depends on the particle size distribution and shape. Spherical particles that are 20 microns and larger are preferable for this process because they tend to flow better and have low internal friction [24]. It was a requirement to achieve at least the near-spherical shape of the particles for easy flow and packing during the sintering process. The potassium bitartrate particles were reduced via a ball milling process and sieved to obtain fine particles for a defined desired particle size and at least near-spherical shape before being coated (Figure 13). This was to also assess the effect each coating formulation has on the particle size and morphology.

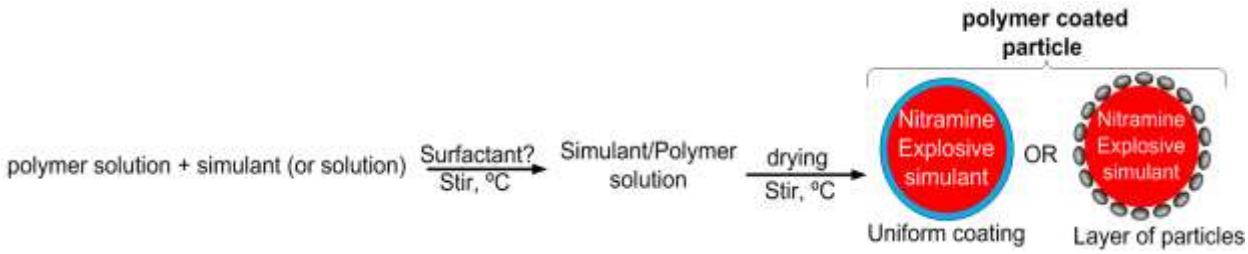

Figure 13: Coating formulation Processes.

3.3 Coating Formulations

3.3.1 Polymer coating of Potassium bitartrate (first rdx simulant)

Mock RDX composites were achieved through co-precipitation via emulsion process [24], seed precipitation [26] and dip coating methods [94]. The formulations evaluated consisted of potassium bitartrate as the RDX simulant (90 % by weight) and a poly-ε-caprolactone and TNT simulants as a binder (10% by weight). The objective was to investigate and evaluate these processes for coating efficiency and their influence on the inert RDX simulant particles with particle size ranging from 50 µm to 200 µm. Parameters such as organic solvent, temperature, pressure and stirring mechanism were varied to find suitable constraints for the required end product. For each experiment, the requirement for the RDX simulant was for it to not dissolve or at least to dissolve slightly in water, and not dissolve at all in the polymer binder medium. For the preparation of microspheres or microcapsules by solvent evapouration or extraction in a oil-to-water emulsion or suspension system, a broad range of substances such as poly(vinyl alcohol) (PVA) are empirically known to be effective.

Mock RDX composites were achieved through co-precipitation via emulsions based processes, seed precipitation and dip coating methods. The formulations evaluated consisted of potassium bitartrate as the RDX simulant (90 % by weight) and a poly-ε-caprolactone as a binder (10% by weight). The objective was to investigate and evaluate these processes for coating efficiency and their influence on the inert RDX simulant particles with particle size ranging from 50 µm to 200 µm. Parameters such as organic solvent, temperature, pressure and stirring mechanism were varied to find suitable constraints for the required end product.

For each experiment, the requirement for the RDX simulant was for it to not dissolve or at least to dissolve slightly in water, and not dissolve at all in the polymer binder medium. The samples presented in this dissertation were achieved using the parameters summarised in Table 1. Dichloromethane was used as the solvent for the binder for all the formulation processes. Figure 14 shows a proposed schematic diagram for the preparation mechanism of the coated RDX mock through selected formulation methods. The protocols for the formulations are described in appendix A. The uncoated and coated powder is appended in Appendix B.

Table 1: Formulation parameters used.

Parameters	Seed precipitation	Dip coating	Co-precipitation
Solvent for simulant	-	-	Acetone
Temperature (during process)	23 °C	23 °C	23 °C
Stirring rate (rpm)	~250	-	8000 (homogeniser)
Surfactant (2 ml)	With and without Surfynol	Surfynol	Surfynol
Solvent evapouration method	23 °C	Fume hood vacuum	Spray dry
Drying time	~24 hours	~2 hours	~45 minutes

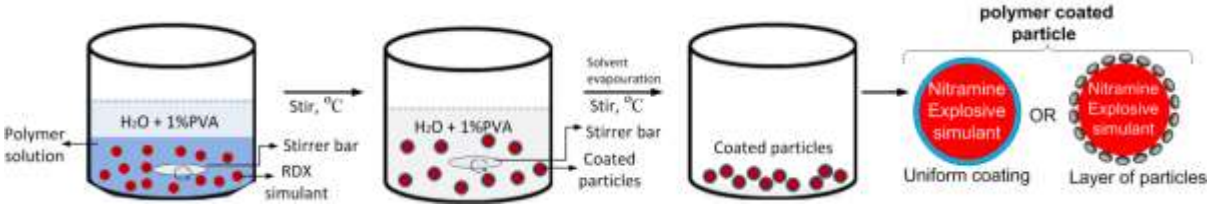

Figure 14: Coating method for a seed precipitation process.

3.3.2 Uniform blend of powders

The powders were mixed in ratios of 90% simulant (80 &100 µm) and 10% PCL, and sintered. This was to achieve the binding process in situ while forming a desired 3D printed layer of simulant as presented in

Figure 15.

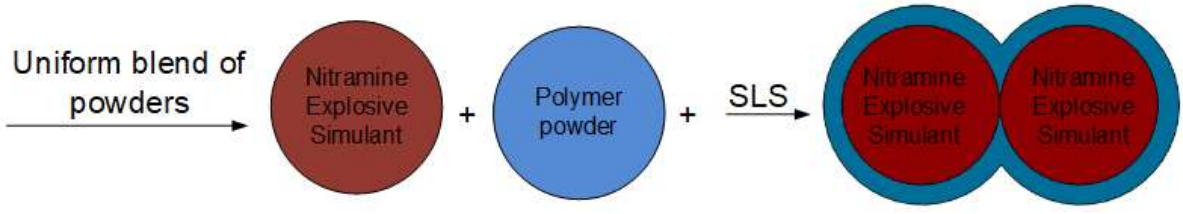

Figure 15: Schematic flow diagram for in situ coating and sintering of blended powders.

3.3.3 Microencapsulation with PCL and TNT simulant

Inert mock RDX composite particles were obtained via emulsion-based processes as shown on the flow diagram in Figure 16. The formulations evaluated consisted of potassium bitartrate as the RDX simulant (90 wt.% and 60 wt.%). The poly-ε-caprolactone was used as a polymeric binder (10 wt.%) and 3,4,5-trimethoxybenzaldehyde was used as TNT simulant as an alternative second binder (40 wt.%). The objective was to investigate and evaluate these processes for their ability to yield the required spherical micro-particles in the desired size range at high coating efficiencies. Parameters such as the nature of the organic solvent, temperature, pressure, stirring intensity and evaporation method were varied to find suitable conditions for the required end product.

A literature procedure [28-29] was employed to effect the microencapsulation of the RDX simulant with PCL. The suspension system procedure is shown schematically in Figure 16 (a). A 100 mg PCL was dissolved in 20 mL DCM, forming a polymer solution. The RDX simulant powder (900 mg) was dispersed into the PCL solution with stirring maintained at 100-200 rpm. This suspension was stirred into a medium made up of 2 mL of the 1 wt.% PVA (used as an emulsifying agent) and 20 mL deionised water. The PVA was utilised to prevented agglomeration of the droplets in the suspension. The resultant suspension was held at 40 ºC and stirred continuously for 6 h. During this time the organic solvent was evaporated and the droplets solidified. The resulting microspheres were recovered from the mixture by decanting and dried in an oven at 40 ºC for about 24 h.

On the other hand, the microencapsulation of the RDX simulant with the TNT simulant was conducted via a single emulsion process, as shown in Figure 16 (b). The TNT simulant was melted by heating to 90 °C. Then the RDX simulant particles were dispersed into the melt by homogenising at 800 rpm for 2 min. The emulsification was achieved using IKAT25 Ultra-Turrax homogeniser. 40 mL deionised water was added while maintaining the temperature at around 90 °C at a reduced stirring speed of ca. 200 rpm for 10 min using a magnetic stirrer. The temperature was then reduced to 23 ºC with stirring for 30 min to obtain droplet microspheres suspended in cooled water. The microspheres were dried in the oven at 50 °C for about 8 h to remove residual water.

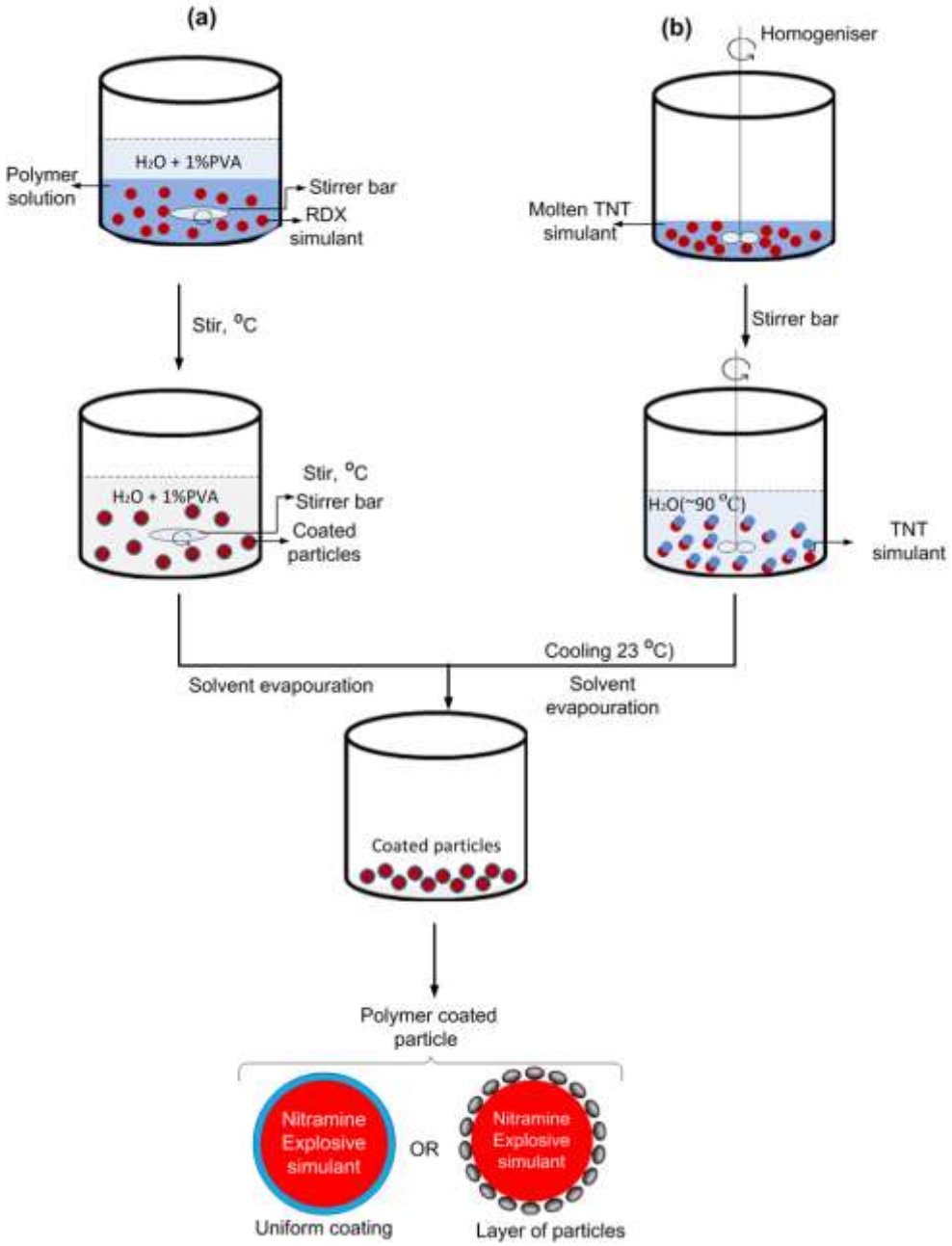

Figure 16: Schematic of the emulsion-based microencapsulation procedures used for the preparation of microspheres: Potassium bitartrate as RDX simulant with (a) 10 wt.% poly(ε-caprolactone) as binder, and (b) 40 wt.% 3,4,5-trimethoxybenzaldehyde as TNT simulant.

3.3.4 Polymer coating of DL-tartaric acid (second rdx simulant)

To coat dl-tartaric acid as, same procedures described in sections 3.3.1 and 3.3.3 were followed. Unfortunately, this simulant was deemed not a good mimic for RDX as it slightly dissolved in water and some organic solvents, and hence discarded for the SLS trials. The results for this simulant are not presented.

3.4 Characterisation

The particle size and morphology were investigated by imaging on a Zeiss Crossbeam 540 FEG Scanning Electron Microscope (SEM) operated between 1kV to 3 kV. Attenuated total reflection-Fourier transform infrared spectroscopy (ATR-FTIR) spectra were recorded on a Perkin Elmer Spectrum 100 Series instrument. The recording was done at 32 scans over the wavenumber range 500–4000 cm^{-1}.

High-resolution confocal Raman imaging was carried out using a WITec alpha300 RAS+ confocal Raman microscope and a 532 nm excitation laser at low power of 1 mW. The surface image scans were acquired using a 50×/0.75 Zeiss objective which gives a diffraction limited lateral resolution of 433 nm, and the scans were acquired over 40 × 40 μm^2 area with 150 points per line and 150 lines per image using an integration time of 1 s.

Differential scanning calorimeter (DSC) runs were conducted on a TA Q100 instrument under a nitrogen atmosphere. The temperature was scanned from -80 to 100 ºC at a ramp rate of 10 ºC/ min. This was done to determine the thermal attributes of the coatings present on the samples, i.e. the melting point, enthalpy change and crystallinity on the coated samples. Laser sinterability was explored with a Synrad CO_2 Infrared (IR) laser (model D48-2-28w). The laser wavelength was 10.6 μm with maximum power of 31 W. The spot size was 2 mm, and the laser power was varied from 0.5 to 3 W.

3.5 Pre-placed Selective Laser Sintering

In SLS applications, a concentrated beam of radiation is created through use of a laser. Two methods were explored to assess the possibility of the materials being sintered via Selective Laser Sintering; (1) to sinter the formulated polymer coated simulant candidates and (2) to sinter a blend of simulant and polymer powders in ratios.

The possibility of a selective laser manufacturing technology on the PCL-coated simulant crystals and uniform blend of powders was conducted with the use of IR laser with about 2 mm spot and maximum output power of 31 W. A pre-placed direct laser sintering process was used, set-up diagram shown in Figure 18. The setup was on a table. Focus mirrors were utilised to direct the laser beam towards the sample (Figure 18). The polymer and simulant were tested separately first, varying the laser power and exposure time and as one sample thereafter. The intentions were to melt the polymer

as a thin film while not melting the simulant crystals inside. Meaning, the aim was for the polymer to absorb the laser energy and melt, and the simulant crystals transmitting the energy thereby sintering and bonding the crystals together at cooling. Therefore, the power and exposure time were varied between 0.5W to 3 W to ensure that the binder does not decompose while sintering. This aim was achieved at 0.5 W laser power, working distance of about 1 m through a laser glass and at determined exposure.

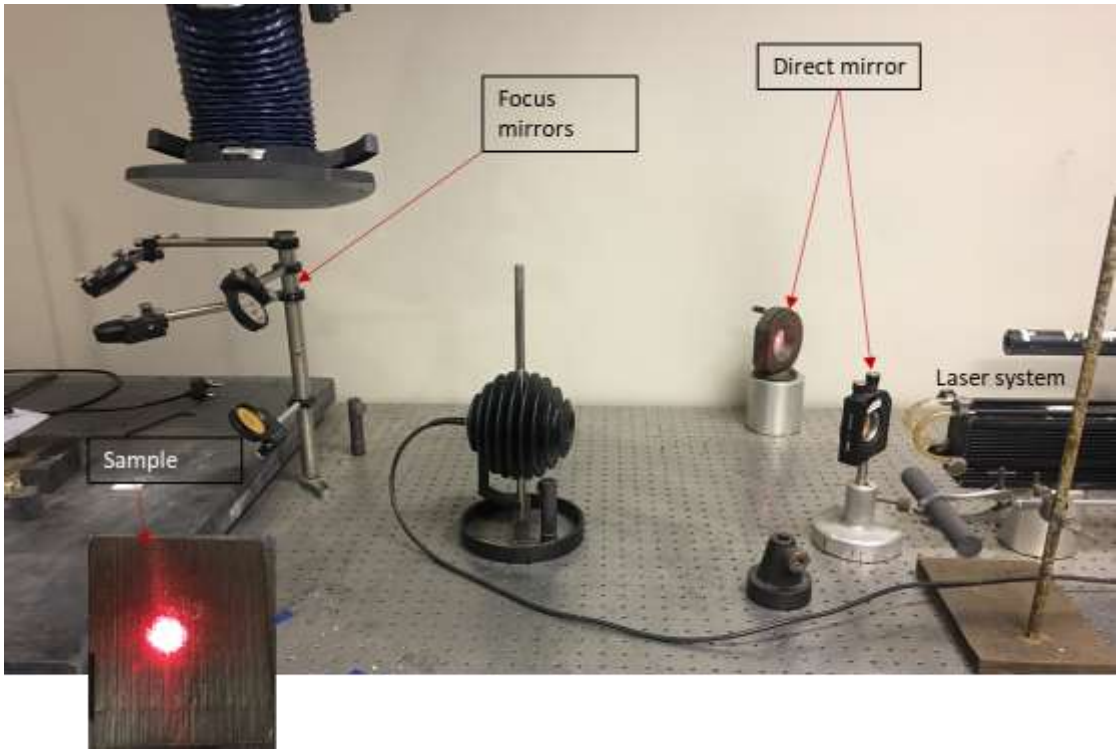

Figure 17: Preplaced SLS experimental set-up.

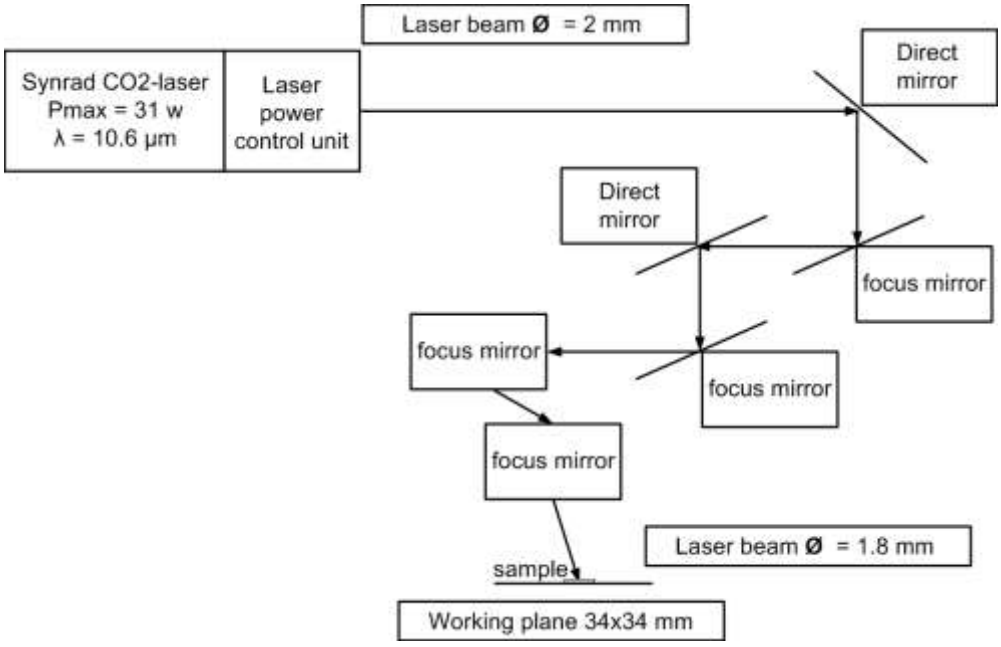

Figure 18: Pre-placed direct laser sintering set-up (not to scale).

3.6 Concentrated solar SLS

Because Fresnel lenses can be used to replace the laser even though they concentrate radiation in a completely different manner. Although lasers can function on low currents, through implementation of a Fresnel lens this part of the process can be made completely sustainable. While the intensity of a laser source is usually described as a Gaussian relationship with regards to distance from the centre of the beam [95], the ideal intensity of a lens is uniform across the focal point. However, because of the inability to create an ideal lens, it is expected that, through defects, the intensity of a radiation concentrated by a Fresnel lens will have a similar distribution.

The experimental setup of the concentrated solar SLS is reported by [96]. As can be seen in Figure 19, the concentrated solar is first harnessed by the solar panel. The Fresnel lens has an aperture diameter of 470 mm and concentrates the solar energy onto a focal spot of roughly 3 mm. This gives the lens a concentration ratio of roughly 24 500. The focal length of the Fresnel lens was determined to be 46 cm.

Because of possible misalignments of the collimating mirror it was decided to suspend the printer from four threaded rods inside the tower as opposed to merely placing it on the floor. This allowed the printer to be adjusted in all directions in order to optimise the size of the focal point. While the x- and y-axes are automatically controlled by the micro-controller, to control the printer in the z direction the threaded rods have to be adjusted manually. This is necessary due to the incoming radiation having a 'conical' profile. Unlike a conventional SLS printer, by adding layers without adjusting the height between the bed and the lens, the incoming energy density would be reduced. A ray-tracing schematic, showing the path of the light is shown in Figure 20.

Figure 19: Designed 3D printer mounted in concentration platform [96].

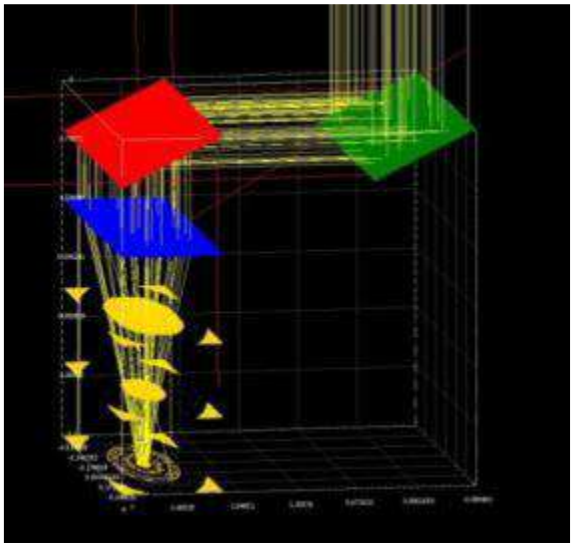

Figure 20: Ray Tracing Schematic of Solar Collector [96].

3.6.1 Testing Procedure

The first step was to characterise the concentrating platform in terms of the amount of radiation it received and how efficiently it is able to concentrate this radiation. This was done on cloudless days as the printer can only be operated at reasonably high direct normal irradiations (DNI). To allow the testing of various factors on the process the predictive salt model was employed in order to generate salt mixtures that mimicked the properties of materials commonly employed in the SLS process. The model was first verified against data from literature in order to ascertain its applicability.

Only 2D tests were conducted. This was to determine the validity of the developed models. The tests were conducted by depositing a powdered material with a known mean particle size onto the movable bed and scanning over the powder at a predetermined velocity. Once this had been done the samples

were cooled to ambient conditions and then analysed. The results were then used to evaluate the model and determine a suitable tuning parameter. This was then used to develop the process control scheme.

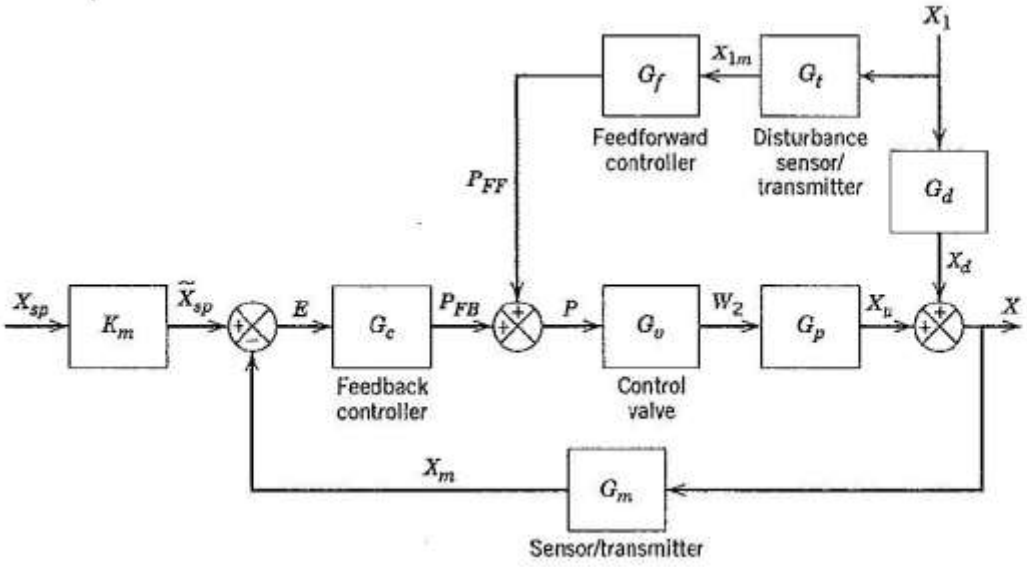

Figure 21: Block-flow diagram for feedforward-feedback control [96].

4 Results and Discussion

4.1.1 Polymer coating of Potassium bitartrate (first rdx simulant)

Figure 22 shows the uncoated simulant used in the formulations with a narrow particle size distribution and with a reasonable Malvern particle sphericity after sieving. The order of sphericity (roundness) of the sieved uncoated particles is demonstrated in Figure 22 (b). The analysis was conducted using a Malvern particles morphology. The closer to the order of 1 the particle gets, the closer it is to a spherical shape. As can be seen in Figure 22 (c), the exact sphericity is not easy to achieve and this challenge is addressed in the literature [7]. Figure 23 shows the Scanning Electron Micrographs of the coated particles achieved from the three coating methods, showing the agglomerated near spherical morphology required. Because the interest lies in the particle shape, size and coating, the images are shown at different magnifications for clarity.

The particle size distribution obtained from the seed precipitation is in the expected micron range (50 <μm> 180), a comparable size to the RDX production grade (A) as a fine crystalline material [18-19,28-29]. The particles from the seed precipitation process were observed to have a uniform coating. For the dip coating method, the coated particle size ranged from 50 μm to 500 μm. The dip coating process (with 1 drop surfactant) gave inconsistent and varying coating on the particles (some particles significantly coated while the others were very thinly and some not coated). This is possible due to the fact that some particles might have been under the others and therefore not getting sufficient exposure to the polymer solution during the dipping process. These parcticles were not satisfactory as some of them agglomerated. For the co-precipitation method, the particles were observed to be thinly coated uniformly but reduced to the nano-size range (200 <nm> 400). This particle size is comparable to the nano-crystalline RDX-based composites found to possess better explosive performance as reported in the literature [7,10,30-31]. This particle size outcome was not the desired one.

It is reported that very-fine particles of RDX explosive are more uniform than larger ones [18]. Therefore, this process could be good for the SLS for controlled packing during fabrication and accurate estimation of density. Additionally, individually coated particles decrease sensitivity and smaller explosive particles organised into clusters that maintain the same structure drastically increase weapon safety and performance [20]. The electrostatic discharge (ESD) values may be greatly influenced by the particle size. The ultrafine particles (<5 μm) have a very large active surface which is negatively charged resulting in a serious electrostatic safety problem. However, this challenge can

be accounted for using a polymeric binder or wax to desensitise the particles [19-25]. Figure 23 (d) depicts a TEM image with a measured coating thickness of 11 nm, sufficiently thin not to affect the hot spots and explosive reactivity. Interestingly, the seed precipitation and co-precipitation formulations seemed to be promising processes regardless of the reduced particle size on the latter process. Additionally, larger particles are easier to spread but fine powders have the potential advantages of increased sinterability, lower surface roughness, thinner layers and aid in the production of more homogeneous parts [27]. Nonetheless, further processes had to be evaluated.

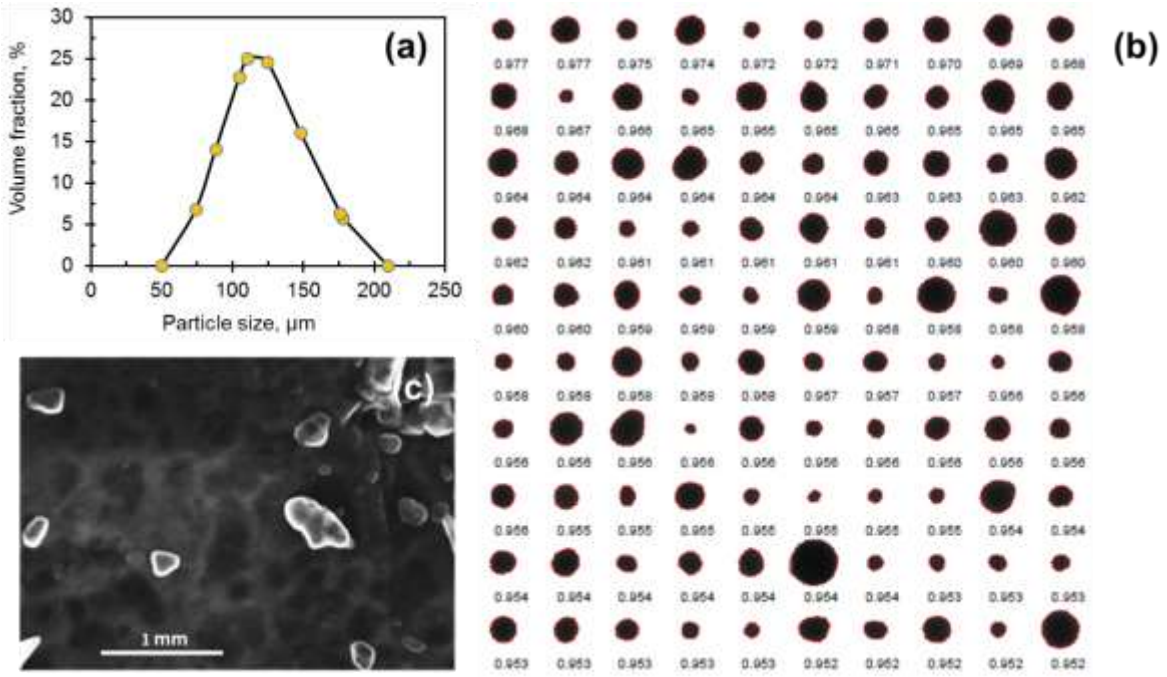

Figure 22: Uncoated RDX simulant (Potassium bitartrate): (a) Particle size distribution, (b) SEM images showing the particle morphology, and (c) Malvern particle Sphericity.

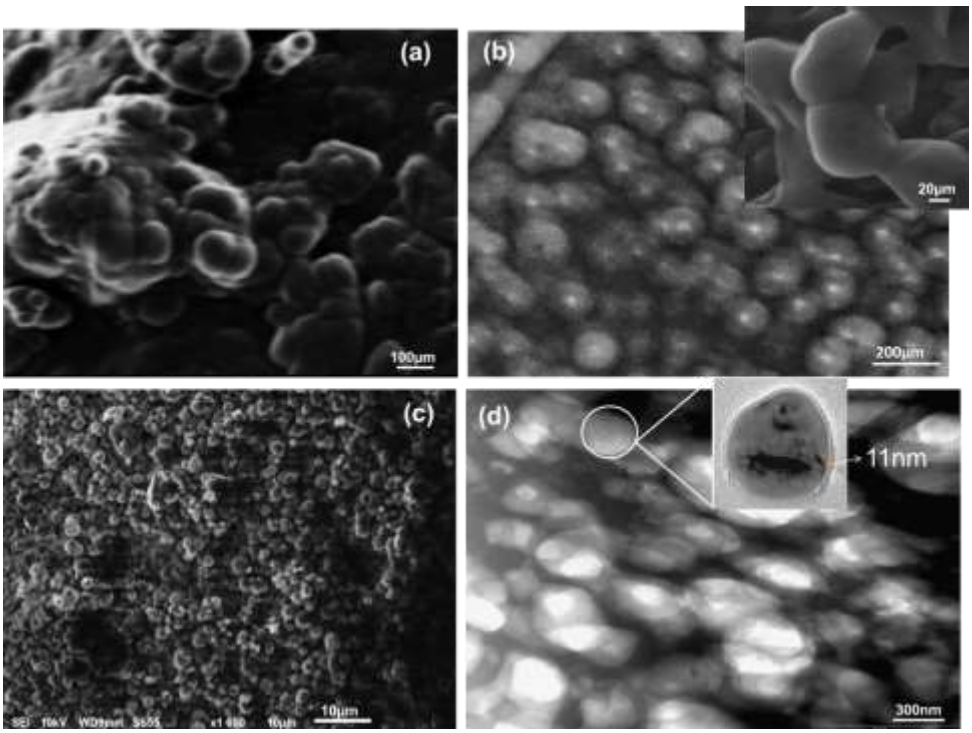

Figure 23: SEM images showing the morphology of the coated particles from (a) dip coating, (b) seed precipitation (c) co-precipitation, and (d) TEM image of the coated particles via co-precipitation.

4.1.2 Suspension and single emulsions (with PCL and TNT simulant binders)

Figure 24(a) shows SEM micrographs of PCL coated particles, obtained with the suspension method. The coated particle size ranged from 50 μm to 500 μm, i.e. it was comparable in size to RDX production grade (A) as a fine crystalline material as reported in the literature [33-34]. To determine the coating thickness, the coated particles were imbedded by Resin on a substrate. An Ultra-microtome cutting method was used to section the coated particles in half. The micrograph of a cross-sectioned particle is shown in Figure 24 (b) with details of the core material and the coating forming the outer shell (thickness around 7 mm).

Figure 25 shows the TNT simulant coating on the RDX simulant particles. Because the interest lies in the particle shape, size and coating, the images are shown at different magnifications for clarity. The particle size ranged from 50 μm to 700 μm. The particles featured a near-spherical morphology with a rough but uniform surface. It can be observed that the microgranule consists of a cluster of smaller particles. Such structural configuration is evidence that the granules formulated possess compact smaller particles with fairly low porosity. This is a potential good application for firepower, as it is reported that individually coated particles decrease sensitivity and smaller explosive particles organised into clusters that maintain the same structure drastically increase weapon safety and

performance [17,22]. Additionally, larger particles (formed of smaller particles) are easier to spread during SLS and thus potential advantage of increased sinterability and aid in the production of more homogeneous parts [41-42]. Figure 25 (a and b) shows close-up detail of the surface. Figure 25 (c and d) show the confocal Raman intensity mapping acquired from the surface and core of the RDX/TNT mock, respectively.

The mapping was carried out over a large area of 40 × 40 μm^2 and 150 × 150 Raman spectra were acquired over a shift of 0 to 3800 cm^{-1} (see the average Raman spectra in Figure 27(a)). From the average Raman spectrum of the surface and core of the RDX/TNT mock, it can be seen that most peaks overlap. However, the peak at 883 cm^{-1} from the core spectrum does not overlap with those from the surface spectrum of the mock. Similarly, the peak at 1585 cm^{-1} from the surface spectrum does not overlap with those from the core spectrum of the mock. As a result, these peaks were used to distinguish the surface and the core of the RDX/TNT mock and to evaluate the uniformity of the chemical composition of the microspheres, as shown in Figure 25 (c and d).

A nearly uniform intensity of the mapping suggests a uniform chemical composition (phase) of TNT coating on RDX core across the analysed areas of the surface and core of the mock. An observed slight variation in the confocal Raman intensity of the mapping is due to the irregular surfaces of the analyzed areas which cause variation in the microscope focal plane during analysis. It was deducted that the formation of these microspheres depends on the slow rate of stirring (around 200 rpm) and evapouration method. Drying or evaporation temperatures around 40-50 ºC and ambient pressure were the key. The literature [30-31,43] also reports that the stirring speed between 100-250 rpm at evapouration temperatures 40-60°C affects particle size diameter ranging from 20-200 μm for coated microspheres. However, it was noted during the experiment that the slow stirring (100-250 rpm) at temperatures between 40-60°C influences microspheres in the region of 50-700 μm, made of a particle cluster.

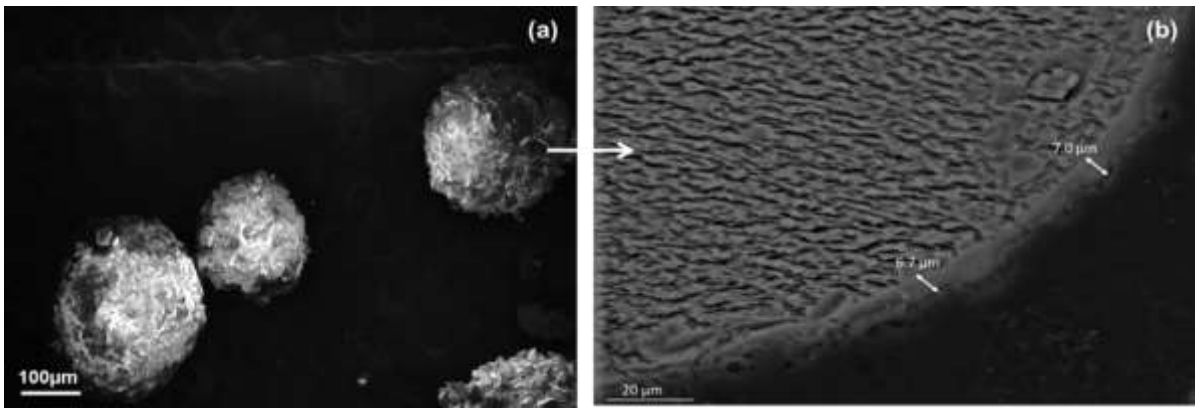

Figure 24: Mock RDX/PCL at magnification (a) and (b) Photomicrograph of coated particle cross-section of the mock showing the coating thickness.

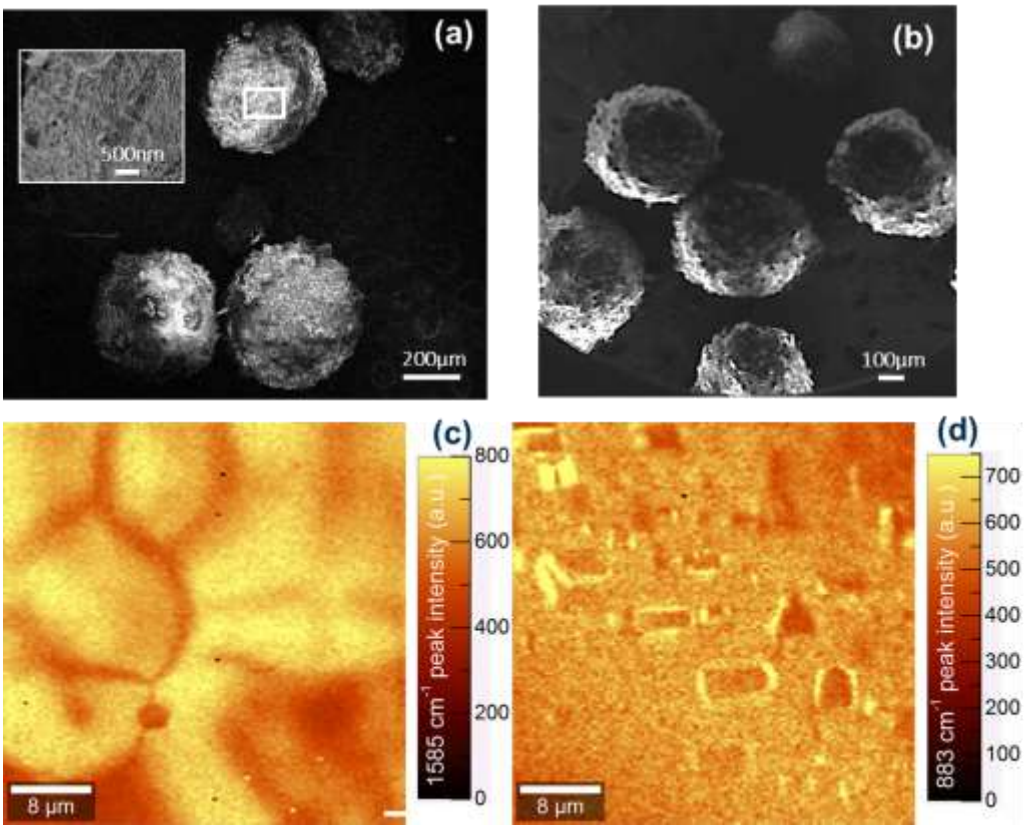

Figure 25: SEM images at low magnification (a) 200 µm, (b) 100 µm, (c) Surface microstructure of the mock RDX/TNT granule, confocal Raman intensity mapping of the 883 and 1585 cm^{-1} peaks of the microsphere (c) core and (d) surface.

FTIR was used primarily to assess and confirm the presence of the binder and to confirm the strong absorbance of the molecules in the coating material at the laser wavelength [15]. It was, therefore, paramount to show the presence of the binder as a coating material in these inert mock composites. Figure 26 (a) and (b) shows the FTIR spectra for the RDX simulant and the coating materials (binders) as references together with the coated samples (inert mock composites). There are some clear

observations that can be made, the peak intensities of the binders' stretching frequencies are comparable with the coated samples.

The peak around 3340 cm^{-1} due to the RDX inert simulant molecule (O-H) is observed on all coated samples and correlates with the mid-IR laser wavelength (2.9 µm). The unique double peak around 2900 cm^{-1} (corresponding to 3.5 µm mid-IR wavelength) due to CH_2 (single peak due to C-H) stretch on both the PCL and 3,4,5-methoxybenzaldehyde spectrum is observed on the coated samples. The simulant also indicates a weak stretching frequency of C-H. The region around 1800 cm^{-1} absorbing area on the coated samples is also observed due to RDX simulant acidic C=O- stretch and a strongly absorbing PCL (ester C=O- stretch). Another strong stretching frequency peaking around 1700 cm^{-1} is due to the TNT inert simulant used as a binder. This is also close to the carbonyl stretching frequency of the RDX simulant. These frequencies correlate to a far-IR laser wavelength (from 5.5 µm) and may not be suitable if the only intention is to activate the binder. Therefore, the best laser wavelength to possibly only activate the binder materials would be around 3.5 µm (due to the CH_2 stretch), the mid-IR laser wavelength.

However, the RDX is reported to be less active and its molecules (such as NO_2, C-H) do not absorb energy in the IR wavelength region. Hence the IR cannot break the chemical bonds of the active molecules to induce the exothermic reaction [72]. From the safety standpoint, this is a good attribute on RDX for the SLS process. Additionally, the RDX does not form a plasma (which may influence ignition of the material) when exposed to energy from the IR wavelengths [44-47]. Therefore, the sintering and fabrication process of active RDX composites may be possible with the whole IR wavelength regime (up to 10.6 µm) as the source of energy.

The chemical vibrational modes were confirmed by the Raman chemical shift analysis, that suggest the similarities of the chemical phases possessed by the coated samples compared to the starting materials. Figure 27 shows the Raman spectra of the starting materials and the mixture (both the mock particle surface and the core presented). The Raman shifts are in agreement with the chemical shifts observed in FTIR spectra. The shifts of the core for the granules seem to be correlating with those of the RDX simulant as highlighted on Figure 27 (a) around 250 cm^{-1}, 900 cm^{-1} and 3000 cm^{-1}. The shifts measured on the coated particle surface compare more with the TNT inert simulant. Figure 27 (b) confirms the uniqueness of the CH_2 shift (2900 cm^{-1}) influenced by the PCL binder observed on all coated samples. There seem to be other common effects around 400-500 cm^{-1} and 2400 cm^{-1} (influenced by O-C=O group) indicating that the coated samples do comprise both starting materials.

It is further observed on the DSC heat curves in Figure 28 (a) that all the coated samples possess an endothermic peak around 60 ºC (absent in the simulant spectrum) due to the melting point of PCL. While Figure 28 (b) shows the thermal attributes on the coated RDX inert simulant particles comparable with 3,4,5-trimethoxybenzaldehyde (TNT simulant). These thermal attributes (endotherm and exotherm) are absent for the neat inert simulant. This confirms the presence of binder materials in the coated samples and that it is possible to activate or soften the binders around their melting points and crystallise at cooling without affecting the simulant. Assuming that the crystallinity of the binder in the coated samples is still the same as before formulation; the binder content is about 9.2% in the sample for PCL -coated particles and about 32% in the simulant TNT-coated particles.

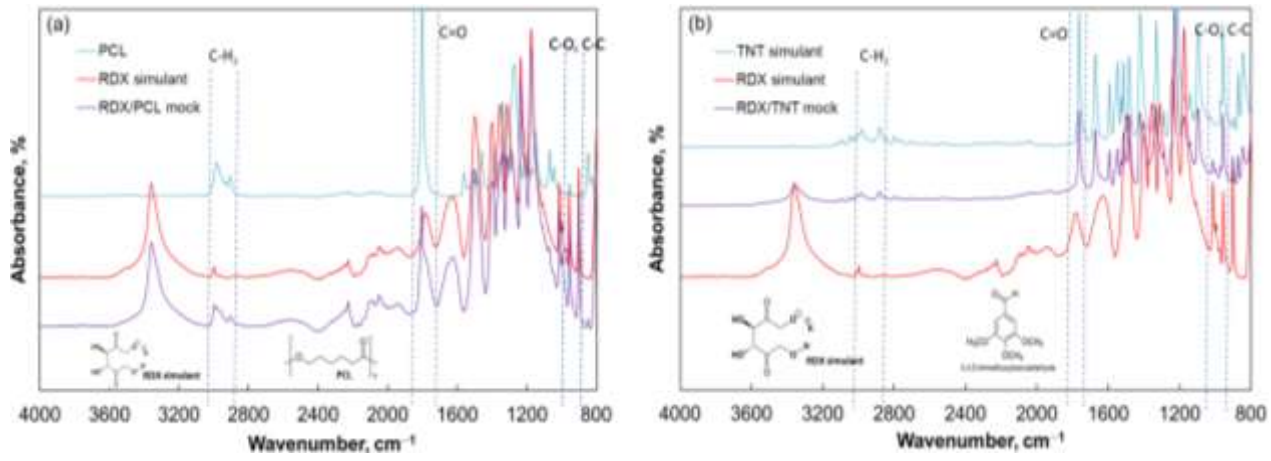

Figure 26: FTIR characterisation of mock explosive formulations.

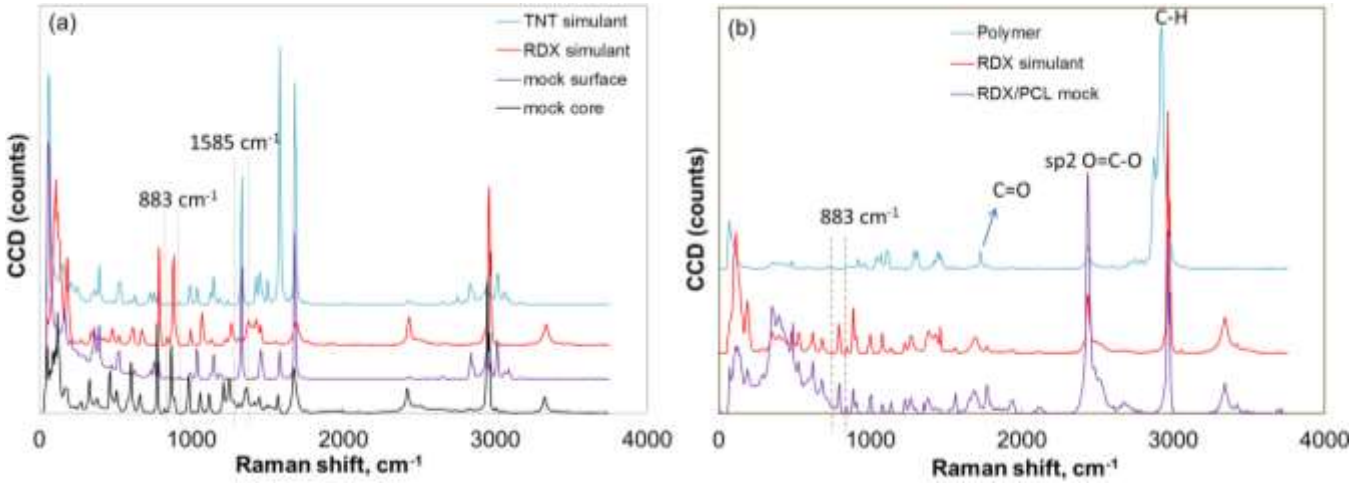

Figure 27: Raman characterisation mock explosive formulations.

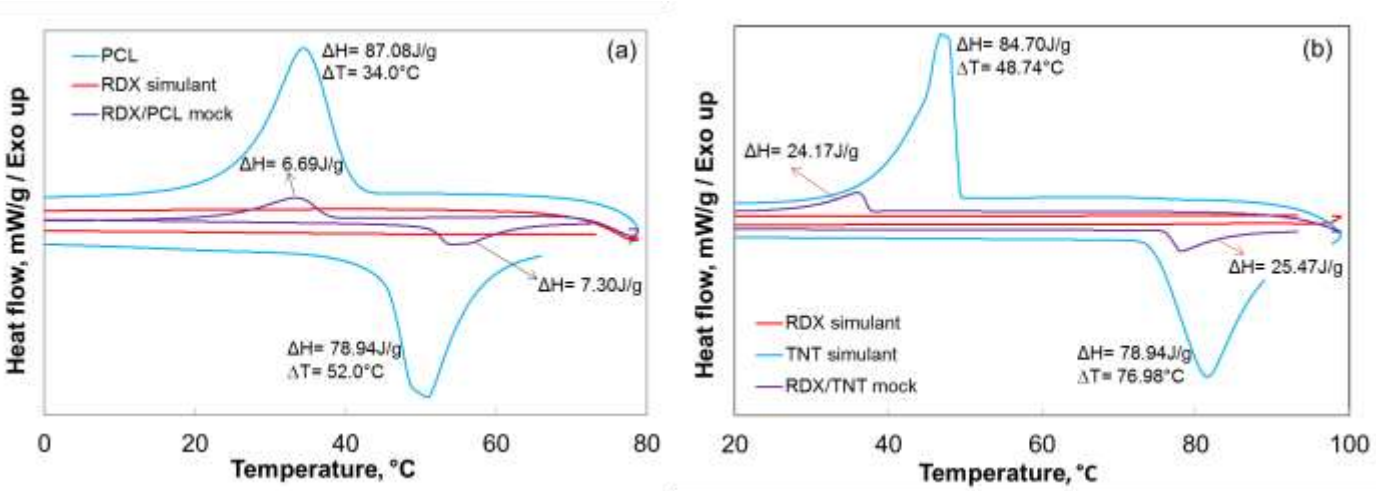

Figure 28: DSC analysis of the HE inert mock composites, (a) PCL coated particles and (b) TNT inert simulant coated particles.

4.2 Selective Laser Sintering tests on coated mock formulations

4.2.1 Seed precipitation, Dip coating and Co-precipitation

Two methods were explored to assess the possibility of the materials being sintered via Selective Laser Sintering;

(1) to sinter the formulated polymer coated simulant candidates,

(2) and to sinter a blend of simulant and polymer powders in ratios.

The possibility of a selective laser manufacturing technology on the PCL-coated simulant crystals and uniform blend of powders was conducted with the use of IR laser with about 2 mm spot and maximum output power of 31 W. A pre-placed direct laser sintering process was used, set-up diagram. The polymer and simulant were tested separately first, varying the laser power and exposure time and as one sample thereafter. The intentions were to melt the polymer as a thin film while not melting the simulant crystals inside. Meaning, the aim was for the polymer to absorb the laser energy and melt, and the simulant crystals transmitting the energy thereby sintering and bonding the crystals together at cooling. This was achieved at 0.5 W laser power, working distance of about 1 m through a laser glass and at the exposure time of 15 s.

The formulated simulant/polymer powders were sintered to assess the viability of the inert RDX simulant particles being fused and packed by a polymeric binder via the SLS method. The possibility of a selective laser manufacturing technology on the PCL-coated RDX simulant particles was conducted on a pre-placed direct laser sintering process, the schematic diagram of the set-up and process is shown in Figure 18 and Figure 29. The aim was for the binder to only absorb the laser energy and get activated to allow coalescence and sintering at cooling. This was achieved from 0.5 W to 3 W IR laser power with a focused beam of about 1.8 mm spot size. The first sintered thin layer was formed and characterised.

Figure 30 demonstrate a single layer of the sintered polymer bonded (cluster) particles. It can be observed in Figure 30 (a and b) that the fusion between the particles obtained via the seed precipitation and dip coating was well facilitated but with voids present. The binder is still observed to be uniform on the layer for the seed precipitation in Figure 30 (a) than the dip coating, Figure 30 (b). The interior void spaces are confirmed on the sintered mock from both the seed precipitation and dip coating processes. These voids may affect the explosive performance (density) of the actual active end product depending on the particle size relative to the void size. Smaller voids relative to the solids should not be a critical factor in explosives. However, it is reported that large structures of RDX without voids do not allow sufficient hot spots for a shock stimulus to generate the conditions needed to start and sustain a chemical reaction [22], hence the voids can be allowed on condition that they are smaller relative to the EM particles.

The density of PCL bonded RDX was estimated from the theory of random packing of spheres [32], to be around 1.57 g/cm^3, comparable to 1.57 g/cm^3 and 1.58 g/cm^3 of C4 and PE4 as a PBX produced from a traditional press powder method. The mock composite (simulant/PCL) density was calculated using the rule of mixtures to be about 1.20 g/cm^3 [33]. Figure 31, on the other hand, shows the sintered area in different magnifications from co-precipitation to give detail to the contact between fused particles, voids and the thin coating. A good bonding and packing of the particles with virtually no voids are observed. The sintered layer was observed to have a homogeneous smoother surface compared to the layers from the seed precipitation and dip coating formulations. This result is influenced by the smaller coated particles (nanoparticles) produced and fused together, forming an intimate cluster. A good packing density and explosive performance of the end product is more possible on nanoparticles as opposed to larger particles [7,10]. The packing density of the PCL bonded RDX nanoparticles is estimated from the theory of close packing of spheres [34] to be about 6% higher than that of micro-particles.

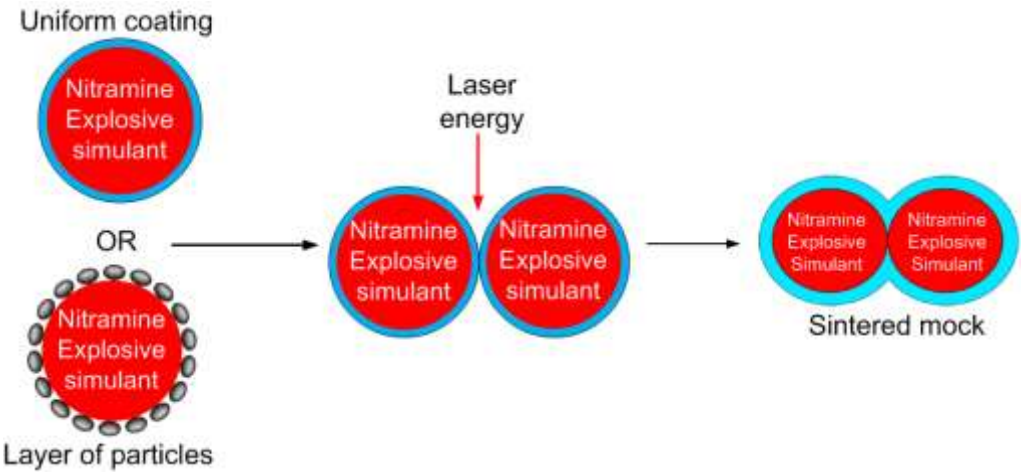

Figure 29: Schematic flow towards binding of coated particles through SLS.

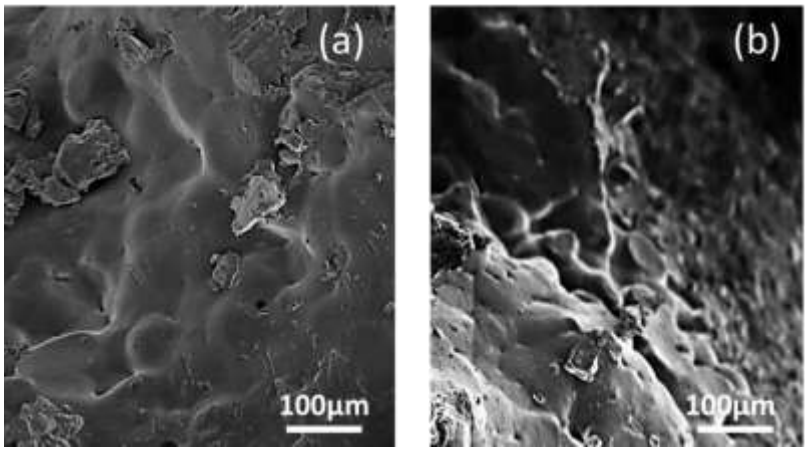

Figure 30: SEM images of a sintered mock (layer) from (a) seed precipitation and (b) dip coating process.

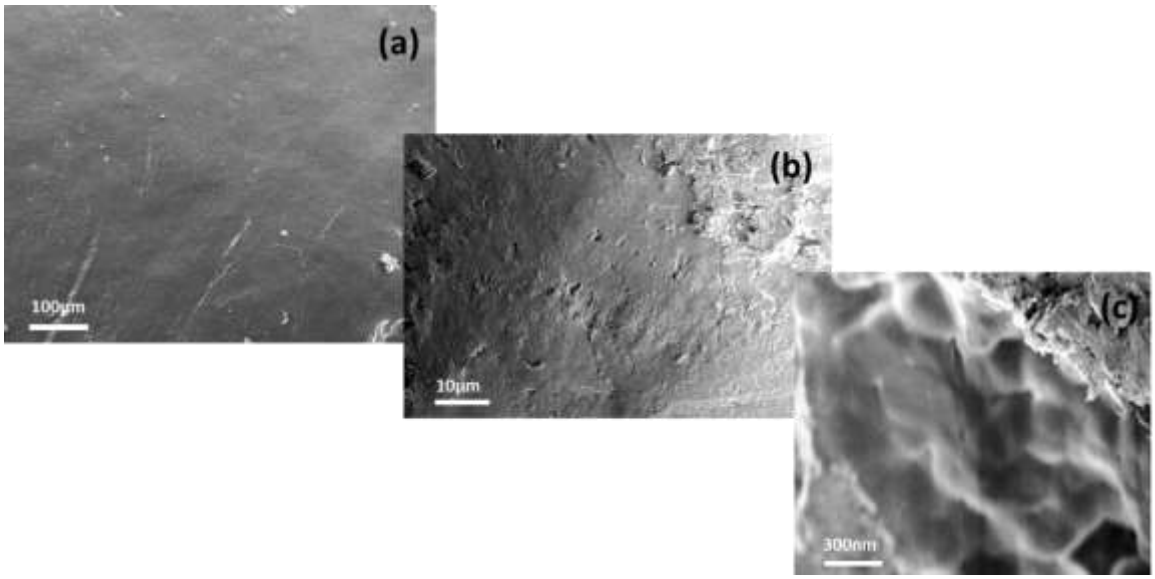

Figure 31: SEM images of a sintered mock (layer) from co-precipitation process at magnifications (a) 100 µm, (b) 10 µm and (c) 300 nm.

4.2.2 Uniform blend of powders

Figure 32 shows the sintered laser of the blend of powders (90%:10%) by mass. The sintering of blended powders did not work well. This may be due the mixing mechanism used.

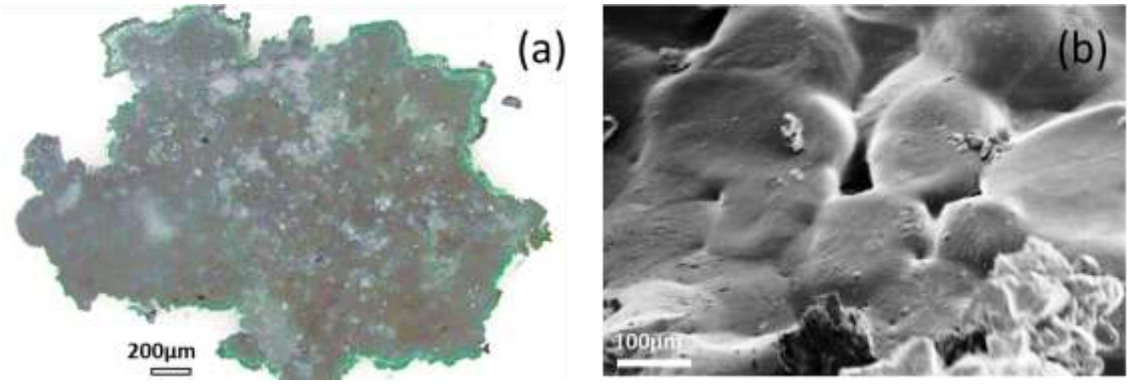

Figure 32: Sintered powder blend of RDX/PCL mock (a) optical micrograph, micrograph. (b) SEM.

4.2.3 Coated particles from Suspension and single emulsion methods (PCL and TNT simulant)

The formulated mocks were sintered to assess the viability of the inert RDX simulant particles being fused and bonded by a polymeric binder and TNT simulant via the SLS method. This was conducted on a pre-placed direct laser sintering process. The aim was for the binder to only absorb the laser energy and get activated to allow coalescence and sintering at cooling.

Initial studies were performed on the binder particles to show that they can indeed absorb the IR wavelength and that it is actually possible to perform SLS. The optical micrographs of the sintered layers are shown in Figure 33 (a) and (b). Figure 33 (c) shows the sintered area, giving details to the contact between bonded particles, voids and the thin coating. The voids observed do agree with the estimation particle packing theory presented in section 2.9.6. It can be observed that the bonding between the PCL-coated particles was well facilitated. It was anticipated that the formulation methods may either produce a uniform coating or a layer of particles. It was then observed that the coating on the surface is uniform and not in a form of “layer of particles”. Hence the effect of the latter was not

determined. Moreover, the uniform coating does influence a good sintering mechanism. The interior void spaces are confirmed on the sintered mock.

These voids may affect the explosive performance (density) of the real active end product depending on the particle size relative to the void size. Smaller voids relative to the solids should not be a critical factor in explosives. However, since it is reported that large structures of RDX without voids do not allow sufficient hot spots for a shock stimulus to generate the conditions needed to start and sustain a chemical reaction [27]; hence the voids can be allowed on condition that they are smaller relative to the EM particles. Additionally, during SLS printing, there must be enough binder to fill the open spaces between closed packed core particles. Otherwise, the overall component will not be void free.

Hence the presence of voids is inevitable with a small binder ratio in the formulation. Increasing the inert binder (polymer) may, however, decrease the performance of the active core. For the PCL coated particles, the sintering was achieved from minimum 0.5 W IR laser power with a focused beam of about 1.8 mm spot size at minimum exposure time of 15 s. This exposure time was validated sufficient to facilitate the bonding between the coated particles without decomposing the polymer. The testing of sufficient power was functional from minimum laser power 0.5 W to 3 W and 15 s exposure time. The polymer was only observed to decompose at higher laser power above 3W for longer exposure times. However it is understood that the laser power does fluctuates at lower powers around 0.5 W. Hence the power should be above 0.5 W. The sintered layer appears to possess a homogeneous smoother surface compared to prior sintering.

Nevertheless, the mock RDX/TNT did not sinter using the IR wavelength. This is possibly due to the TNT simulant absorbing energy insufficiently around the wavelength used. Moreover, when exposed to the solar energy SLS, it still did not sinter but the coated particles decomposed around 150 ºC, as can be observed in Figure 33 (d). In solar energy SLS, The SLS system used the energy harnessed form the solar radiation as the source of energy to sinter the material. The sun rays were concentrated and focused with a Fresnel lens. It was then concluded that the TNT simulant is not suitable for SLS as the AM technique, and hence the real TNT may not be conducive for this technique environment. Therefore, another AM technique should be considered for this formulation.

The packing density of both mock composites was calculated using the rule of mixtures and it is estimated to be 1.20 g/cm^3 [24]. The density of PCL-bonded real active RDX was estimated from the theory of random packing of spheres [100], to be around 1.57 g/cm^3, comparable to that of C4 and PE4 as a PBX produced from a traditional press powder method. The density of TNT-coated RDX was also estimated around 1.64 g/cm^3 which also comparable to that of composition B explosive mixture. For this proof of concept, only one sintered layer was formed as a pre-placed sintering

method (manual) was used. Determination of the packing density, experimentally, shall be conducted in the follow-up study on optimization of these methods on active materials.

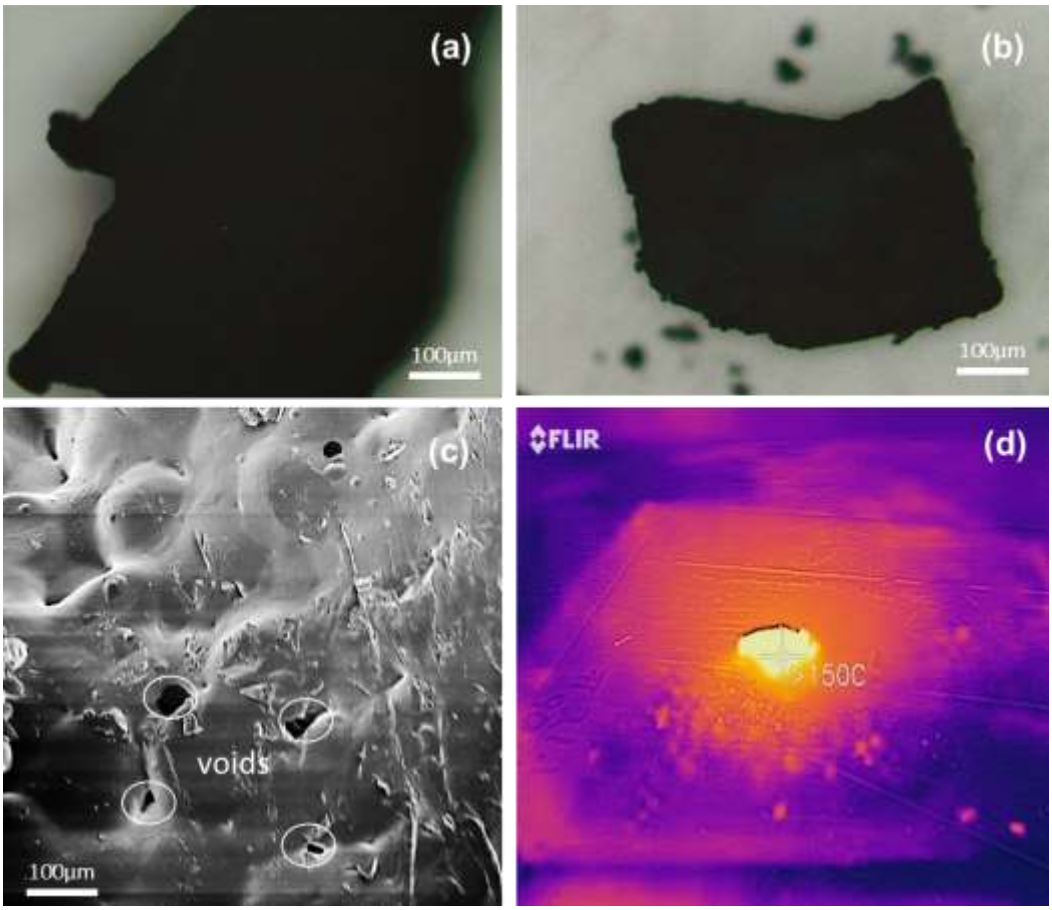

Figure 33: (a) and (b) Optical micrograph of a sintered PCL and TNT simulant, (c) SEM images of sintered mock (layer) from PCL coated RDX simulant particles, (d) High speed image of RDX/TNT mock showing the decomposed TNT simulant area after exposure to solar energy SLS.

5 Conclusion

The purpose of this project was to investigate and evaluate coating processes to enable SLS of energetic material composites. This was primarily conducted through a demonstration of the concept by use of inert simulants and thus mocks for safety and practicality reasons. For this study, coating formulations namely; seed precipitation dip coating and co-precipitation, suspension and single emulsions were investigated for uniform coating effectiveness, required near-spherical particle morphology and micron size range, and bonding performance under a selective laser sintering method. Potassium bitartrate was used successfully as an inert simulant for RDX, 3,4,5-trimethoxybenzaldehyde and polycaprolactone as coating and binders. The seed precipitation was found to produce mock particles with required constraints such as near spherical morphology, expected size range (50 <μm> 180) and uniform coating). However, the unwanted agglomeration on some of the particles was observed. The coating on particles from the dip coating process (with surfactant) was not uniform but with accepted morphology and size. Furthermore, the process gave inconsistent with low repeatable results, hence not acceptable. The co-precipitation gave accepted uniform coating and particle shape but with reduced size (200 <nm> 400), which was the undesired outcome for this experiment.

The suspension system and single emulsion investigated (varying the input parameters for PCL and TNT simulant) resulted into required de-agglomerated coated microspheres, uniform coating effectiveness and bonding under a selective laser sintering method. The resultant PCL coated microspheres possessed a uniform coating. The microspheres coated with inert simulant TNT comprised compact particles and uniform coating with fairly rough surface. Both the suspension and single emulsion processes were found to produce mock powder particles with required constraints such as spherical morphology, required size range (> 20μm) with uniform but rough coating surface. The SLS concept was demonstrated successfully for the PCL coated mock. Preliminary binding experiments indicate that laser sintering with IR wavelength for PCL coated RDX simulant particles from the suspension process is plausible according to the bonding mechanism of the coated particles regardless of the voids formed. On the other hand, the TNT inert simulant coated RDX simulant (RDX/TNT mock) is found to be incompatible and unsuitable with the SLS technique.

It is therefore recommended that non-laser energy based additive manufacturing techniques such as binder jetting be tried for this formulation. Further research within this project aims to investigate the suspension and single emulsion processes as coating formulations with already determined parameters using the actual active RDX and further characterise the composites for performance and

safety for the SLS. The results from this approach will be used to compare with the PBXs from the traditional methods.

6 References

[1] Emery S. REVIEW : Traditional manufacturing of explosives. vol. Distributi. 2015. doi:IHEODTD 16-061.

[2] Thomas M. The Magic of Rapid Prototyping for User Research: Much More Than Smoke and Mirrors. January 30 2014.

[3] Murray AK, Isik T, Ortalan V, Gunduz IE, Son SF, Chiu GTC, et al. Two-component additive manufacturing of nanothermite structures via reactive inkjet printing. J Appl Phys 2017;122:1–6. doi:10.1063/1.4999800.

[4] Brandt M. The role of lasers in additive manufacturing, Laser additive manufacturing. In: Brandt M, editor. Laser Addit. Manuf. Mater. Des. Technol. Appl. 1st ed., Cambridge, United Kingdom: Woodhead Publishing; 2016, p. 1–18.

[5] Cotteleer, Mark, Jonathan Holdowsky MM, Coykendall J. 3D opportunity in a erospace and defense. Deloitte Univ Press 2014.

[6] Lawrence Livermore National Laboratory. 3D Printing of Energetic Materials and Components for Optimized or Enabling Technologies n.d. https://ipo.llnl.gov/technologies/energy_materials.

[7] Gash A. High-Explosive Components Using Advanced Manufacturing Methods. Lawrence Livemore Natl Lab 2015.

[8] Hutterer E. Explosives 3D Printing 2016:2–5. https://www.lanl.gov/discover/publications/1663/2016-march/_assets/docs/1663_26_explosive-3d-design.pdf (accessed June 27, 2018).

[9] Jeff K. A Look Inside the “Explosive” 3D-Printing Industry n.d. http://www.machinedesign.com/3d-printing/look-inside-explosive-3d-printing-industry (accessed June 27, 2018).

[10] Los Alamos Science and Technology Magazine. 3D-printed explosives Fine-tuning microbial metabolism New tamper-evident seals tell all Breaking bacterial defenses. Los Alamos Natl Lab 2016:2–29.

[11] Saffarzadeh M, James Gillispie G, Brown P. Selective Laser Sintering (Sls) Rapid Protytping Technology: a Review of Medical Applications 2016.

[12] Goodridge RD, Ziegelmeier SZ. Powder Bed Fusion of Polymers. Laser Addit. Manuf. Mater. Des. Technol. Appl., 2017. doi:DOI: 10.1016/B978-0-08-100433-3.00007-5.

[13] Bakshi KR, Mulay A V. A Review on Selective Laser Sintering: A Rapid Prototyping Technology. IOSR J Mech Civ Eng 53 Page MES Coll Eng 2016:2278–1684. doi:10.9790/1684-15008040453-57 LK - https://aus.on.worldcat.org/oclc/6682027765.

[14] Kelbassa I, Gasser A, Meiners W, Backes G, M€uller B. High-speed LAM. 37th MATADOR Conf. Adv. Manuf., UK: 2012, p. 3386.

[15] Ngo TD, Kashani A, Imbalzano G, Nguyen KTQ, Hui D. Additive manufacturing (3D printing): A review of materials, methods, applications and challenges. Compos Part B Eng 2018;143:172–96.

doi:10.1016/j.compositesb.2018.02.012.

[16] Prakash KS, Nancharaih T, SubbaRaoc VV. Additive Manufacturing Techniques in Manufacturing -An Overview. Materialstoday, 2018, p. 3873–82.

[17] Zhu W, Yan C, Shi Y, Wen S, Liu J, Shi Y. Investigation into mechanical and microstructural properties of polypropylene manufactured by selective laser sintering in comparison with injection molding counterparts. Mater Des 2015;82:37–45. doi:10.1016/j.matdes.2015.05.043.

[18] Yuan S, Shen F, Bai J, Chua CK, Wei J, Zhou K. 3D soft auxetic lattice structures fabricated by selective laser sintering: TPU powder evaluation and process optimization. Mater Des 2017;120:317–27. doi:10.1016/j.matdes.2017.01.098.

[19] Yuan S, Shen F, Chua CK, Zhou K. Polymeric composites for powder-based additive manufacturing: Materials and applications. Prog Polym Sci 2019;91:141–68. doi:10.1016/j.progpolymsci.2018.11.001.

[20] Utela B, Storti D, Anderson R, Ganter M. A review of process development steps for new material systems in three dimensional printing (3DP). J Manuf Process 2008;10:96–104. doi:10.1016/j.jmapro.2009.03.002.

[21] Scheck CE, Wolk JN, Frazier WE, Mahoney BT, Morris K, Kestler R, et al. Naval Additive Manufacturing: Improving Rapid Response to the Warfighter. Nav Eng J 2016;128:5.

[22] Hunt EM, Jackson M. Coating and characterization of mock and explosive materials. Adv Mater Sci Eng 2012;2012:5. doi:10.1155/2012/468032.

[23] Elizabeth DCM, Moreira ED, Diniz MF, Dutra RCL, Da Silva G, Iha K, et al. Characterization of polymer-coated RDX and HMX particles. Propellants, Explos Pyrotech 2008;33:44–50. doi:10.1002/prep.200800207.

[24] Staymates M, Fletcher R, Staymates J, Gillen G, Berkland C. Production and characterization of polymer microspheres containing trace explosives using precision particle fabrication technology. J Microencapsul 2010;27:426–35. doi:10.3109/02652040903367335.

[25] Jain RA. The manufacturing techniques of various drug loaded biodegradable poly (lactide- co -glycolide) (PLGA) devices. Biomaterials 2000;21:2475–90.

[26] Arshady R. Preparation of biodegradable microspheres and microcapsules: 2. Polyacides and related polyesters. J Control Release 1991;17:1–22. doi:ADONIS016836599100038u.

[27] PANT A, Amiya KN. Preparation and Characterization of Ultrafine RDX. Cent Eur J Energ Mater 2013;6:19–21.

[28] Trzcinski T, Palka N, Szustakowski M. THz spectroscopy of explosive-related simulants and oxidizers. Bull Polish Acad Sci Tech Sci 2012;59:445–7. doi:10.2478/v10175-011-0056-4.

[29] Ahmad RS, Cartwright M. Laser ignition of energetic materials. WILEY, 2014, p. 256–8.

[30] Spahlinger G. Recent Advances in High Nitrogen Energetic Materials Energetic Materials In Daily Life 2014:63.

[31] Tlapotke T. Chemistry of High Energetic Materials. Gruyter Textb 2012.

[32] Akhavan J. Introduction to Explosives. Chem. Explos., Cambridge, UK: The Royal Society of Chemistry; 2004, p. 1–20.

[33] Commercial High Explosives n.d. http://www.tracefireandsafety.com/VFRE-99/Recognition/High/high.htm (accessed November 22, 2018).

[34] Gao C, Yang L, Zeng Y, Wang X, Zhang C, Dai R, et al. Growth and Characterization of β-RDX Single Crystal Particles. J Phys Chem 2017;121. doi:https://doi.org/10.1021/acs.jpcc.7b04285.

[35] MOLT Jr R w. NITRAMINE CONFORMERS AND DETONATION MECHANISM VIA STANDARD COUPLED CLUSTER AND DOUBLE-ELECTRON ATTACHED COUPLED CLUSTER THEORY. UNIVERSITY OF FLORIDA, 2013.

[36] Figueroa-Navedo AM, Ruiz-Caballero JL, Pacheco-Londoño LC, Hernández-Rivera SP. Characterization of α- And β-RDX Polymorphs in Crystalline Deposits on Stainless Steel Substrates. Cryst Growth Des 2016;16:3631–8. doi:10.1021/acs.cgd.6b00078.

[37] Cyclotrimethylenetrinitramine n.d. http://lem.ch.unito.it/didattica/infochimica/2008_Esplosivi/RDX.html (accessed November 21, 2018).

[38] Strauss B, Cited R, Costigan EF. Process of reducing shock sensitivity of explosive nitramine compounds by crystal modification 1992:6–9.

[39] Gardner AE. Process For Desensitizing Solid Explosive. 3,544,360, 1970. doi:US3544360A.

[40] S. Venkatachalam. G., SanthoshNinan KN, Ninan KN. Introduction to Explosives and Propellants. P1 Int. HEMS1 Work., 2002, p. 87–106.

[41] Weinheime R. Desensitized RDX due to Crystal growth. 27th Int Pyrotech Semin 2000.

[42] Lev P, Njit K. Processing and Characterization of Nano RDX 2009.

[43] Jung W, Park J, Lee W, Lee J, Koo K, Oh M. Scale-Up of a Crystallizer for Production of Nano-Sized Energetic Materials. Chem Eng Technol 2016;39:1309–16. doi:10.1002/ceat.201600027.

[44] Narh KA, Agwedicham AT, Jallo L. Dry coating polymer powder particles with deagglomerated carbon nanotubes to improve their dispersion in nanocomposites. Powder Technol 2008;186:206–12. doi:10.1016/j.powtec.2007.12.004.

[45] Wang P, Shi C, He Q, Xu S. Preparation and characterization of ultrafine CL-20. Huogongpin 2009;6:19–21.

[46] Huang B, Cao M, Nie F, Huang H, Hu C. Construction and Properties of Structure- and Size-controlled Micro/nano-Energetic Materials. Def Technol 2013;9:59–79. doi:10.1016/j.dt.2013.10.003.

[47] Song, Xiaolan and Li F. Dependence of Particle Size and Size Distribution on Mechanical Sensitivity and Thermal Stability of Hexahydro-1, 3, 5-trinitro-1, 3, 5-triazine. Def Sci J 2009;59:37–42.

[48] Kim DY, Kim KJ. Solubility of cyclotrimethylenetrinitramine (RDX) in binary solvent mixtures. J Chem Eng Data 2007;52:1946–9. doi:10.1021/je7002463.

[49] States U, Parrish CF, Haute T, Edelberg F, Robert P, Suga AM. represented by the Secretary of the 1977;38:54–6.

[50] Hildebrant JF, Banker RB. United States Patent [19] 1978:54–5. doi:10.1016/j.scriptamat.2005.10.045.

[51] Marraud C (Chevanceaux), FR) SM (Le H, (Pessac FC, (Begles) CA. Desensitization by Coating Crystals of Explosives Energy Substances, Coated Crystals of such substances, and Energy Materials. US 20100307648A1, 2010.

[52] Fletcher RA, Brazin JA, Staymates ME, Benner BA, Gillen JG. Fabrication of polymer microsphere particle standards containing trace explosives using an oil/water emulsion solvent extraction piezoelectric printing process. Talanta 2008;76:949–55. doi:10.1016/j.talanta.2008.04.066.

[53] Konek C. Terahertz spectroscopy of explosives and simulants: RDX, PETN, sugar, and L-tartaric acid. SPIE Defense, … 2009;7311:73110K-73110K – 7. doi:10.1117/12.817913.

[54] Nampi PP, Kume S, Hotta Y, Watari K, Itoh M, Toda H, et al. The effect of polyvinyl alcohol as a binder and stearic acid as an internal lubricant in the formation, and subsequent sintering of spray-dried alumina. Ceram Int 2011;37:3445–50. doi:10.1016/j.ceramint.2011.05.149.

[55] Campbell MS, Garcia D, Idar D. Effects of temperature and pressure on the glass transitions of plastic bonded explosives. Thermochim Acta 2000;357–358:89–95. doi:10.1016/S0040-6031(00)00372-5.

[56] T.R. Gibbs AP. LASL Explosives Property Data. University of California Press; 1980.

[57] Wang J, Ye B, An C, Wu B, Li H, Wei Y. Preparation and Properties of Surface-Coated HMX with Viton and Graphene Oxide. J Energ Mater 2016;34:235–45. doi:10.1080/07370652.2015.1053016.

[58] Yang Z, Ding L, Wu P, Liu Y, Nie F, Huang F. Fabrication of RDX , HMX and CL-20 based microcapsules via in situ polymerization of melamine – formaldehyde resins with reduced sensitivity 2015;268:60–6.

[59] Thelma G. Manning and Bernard Strauss. Reduction of energetic filler sensitivity in propellants through coating. US 6,524,706 B1, 2003.

[60] Liu J, Jiang W, Yang Q, Song J, Hao G zi, Li F sheng. Study of nano-nitramine explosives: preparation, sensitivity and application. Def Technol 2014;10:184–9. doi:10.1016/j.dt.2014.04.002.

[61] Mattos EC, Diniz MF, Nakamura NM, Dutra R de CL. Determination of polymer content in energetic materials by FT-IR. J Aerosp Technol Manag 2009;1:167–75. doi:10.5028/jatm.2009.0102167175.

[62] An CW, Li FS, Song XL, Wang Y, Guo X De. Surface coating of RDX with a composite of TNT and an energetic-polymer and its safety investigation. Propellants, Explos Pyrotech 2009;34:400–5. doi:10.1002/prep.200700286.

[63] Lu M, Zhou XL. Research on Insensitivity of RDX Coated with TNT. Chin J Explos Prop 2006;29.

[64] Ghosh SK. Functional Coatings: by Polymer Microencapsulation. KgaA, Weinheim: Wiley-VCH Verlag GmbH & Co; 2006.

[65] O'Donnell PB, McGinity JW. Preparation of microspheres by the solvent evaporation technique. Adv Drug Deliv

Rev 1997;28:25–42. doi:10.1016/S0169-409X(97)00049-5.

[66] Stepanov V, Krasnoperov LN, Elkina IB, Zhang X. Production of nanocrystalline RDX by Rapid Expansion of Supercritical Solutions. Propellants, Explos Pyrotech 2005;30:178–83. doi:10.1002/prep.200500002.

[67] Lee B, Jeong J, Lee Y, Lee B, Kim H, Kim H, et al. Supercritical Antisolvent Micronization of Cyclotrimethylenetrinitramin : Influence of the Organic Solvent 2009:11162–7.

[68] Cortopassi A, Adair JH, Essel JT, Cortopassi AC, Kuo KK, Leh CG, et al. Formation and Characterization of Nano - sized RDX Particles Produced Using the RESS - AS Process Formation and Characterization of Nano-sized RDX Particles Produced Using the RESS-AS Process 2012. doi:10.1002/prep.201100139.

[69] Paul Wanninger, Richard Wild, Ernst Kleinschmidt HS. Pressable explosive granular product and pressed explosive charge 1996;US 5547526.

[70] Yadroitsev I, Bertrand P, Grigoriev S, Antonenkova G, Smurov I. Use of track/layer morphology to develop functional parts by selective laser melting. J Laser Appl 2014;25:052003. doi:10.2351/1.4811838.

[71] Yan Z, Zhang C, Liu W, Li J, Huang M, Wang X, et al. Ultraviolet Laser-induced ignition of RDX single crystal. Sci Rep 2016;6:20251. doi:10.1038/srep20251.

[72] Ming-Wei Chen, Sizhu You, Kenneth S. Suslick and DDD. Hot spot generation in energetic materials created by long-wavelength infrared radiation. Appl Phys Lett 2014;104.

[73] Penttilä A, Lumme K. The effect of particle shape on scattering - A study with a collection of axisymmetric particles and sphere clusters. J Quant Spectrosc Radiat Transf 2004;89:303–10. doi:10.1016/j.jqsrt.2004.05.030.

[74] ia, F., Sumi, N., Ishikawa, K., Kano, H., Inui, H., Kularatne, J., Takeda, K., Kondo, H., Sekine, M., Kono, A., Hori M. Laser Scattering Diagnosis of a 60-Hz Non-Equilibrium Atmospheric Pressure Plasma Jet. Appl Phys Express 2011;4.

[75] Laser Diffraction. Malvern Instruments Ltd 2017. https://www.malvern.com/en/products/technology/laser-diffraction (accessed November 22, 2018).

[76] Jiba Z, Focke WW, Kalombo L, Madito MJ. Coating processes towards selective laser sintering of energetic material composites. Def Technol 2019. doi:10.1016/j.dt.2019.05.013.

[77] Stepanov V, Anglade V, Balas Hummers WA, Bezmelnitsyn A V, Krasnoperov LN. Production and sensitivity evaluation of nanocrystalline RDX-based explosive compositions. Propellants, Explos Pyrotech 2011;36:240–6. doi:10.1002/prep.201000114.

[78] Cocchi M, Foca G, Lucisano M, Marchetti A, Paean MA, Tassi L UA. Classification of cereal flours by chemometrie analysis of MIR spectra. J Agric Food Chem 2004;52:1062–1067.

[79] Dowell FE, Maghirang EB, Xie F, Lookhart GL, Pierce RO, Seabourn BW, et al. Predicting wheat quality characteristics and functionality using near-infrared spectroscopy. Cereal Chem 2006;83:529–36. doi:10.1094/CC-83-0529.

[80] Amir RM, Anjum FM, Khan MI, Khan MR, Pasha I, Nadeem M. Application of Fourier transform infrared (FTIR) spectroscopy for the identification of wheat varieties. J Food Sci Technol 2013;50:1018–23. doi:10.1007/s13197-011-0424-y.

[81] Differential scanning calorimetry – a review and what's new. Eur Pharm Rev n.d. https://www.europeanpharmaceuticalreview.com/article/2943/why-is-thermal-analysis-important-to-the-industry (accessed November 12, 2018).

[82] Brown ME. Chapter 4: Differential Thermal Analysis (DTA) and Differential Scanning Calorimetry (DSC) n.d. https://www.globalspec.com/reference/36941/203279/chapter-4-differential-thermal-analysis-dta-and-differential-scanning-calorimetry-dsc (accessed November 21, 2018).

[83] Frank H. Chung. Quantitative Interpretation of X-ray Diffraction Patterns of Mixtures.II. Adiabatic Principle of X-ray Diffraction Analysis of Mixtures. J Appl Cryst 1974;7:526–31. doi:https://doi.org/10.1107/S0021889874010387.

[84] Lutterotti L. X-ray diffraction: theory and applications to materials science and engineering. Mater Sci Eng n.d. http://www.ing.unitn.it/~luttero/phd/C1_crystallography.pd (accessed November 22, 2018).

[85] Szpiro G. Does the proof stack up? Nature 2003;424:12–3. doi:10.1038/424012a.

[86] Song C, Wang P, Makse HA. A phase diagram for jammed matter. Nature 2008;453:629.

[87] Hudson DR. Density and Packing in an Aggregate of Mixed Spheres. J Appl Phys n.d.;20:154–162. doi:https://doi.org/10.1063/1.1698327.

[88] Zong C. From deep holes to free planes. Bull Am Math Soc 2002;39:533–55. doi:10.1090/S0273-0979-02-00950-3.

[89] Abu-lebdeh T, Damptey R, Lamberti V, Hamoush S. Powder Packing Density and Its Impact on SLM-Based Additive Manufacturing. Springer International Publishing; 2019. doi:10.1007/978-3-030-05861-6.

[90] Karapatis N, Egger G. Optimization of powder layer density in selective laser sintering. Int Solid Free Fabr Symp 1999:255–64.

[91] Jacob G, Donmez A, Slotwinski, J and Moylan S. Measurement of powder bed density in powder bed fusion additive manufacturing processes. Meas Sci Technol 2016;27. doi:doi:10.1088/0957-0233/27/11/115601.

[92] O'Toole PI, Hudson TS. New high-density packings of similarly sized binary spheres. J Phys Chem C 2011;115:19037–40. doi:10.1021/jp206115p.

[93] Mokoena EM, Datye AK, Coville NJ. A systematic study of the use of DL-tartaric acid in the synthesis of silica materials obtained by the sol-gel method. J Sol-Gel Sci Technol 2003;28:307–17. doi:10.1023/A:1027418230211.

[94] Schneller T, Waser R, Kosec M, Payne D. Chemical solution deposition of functional oxide thin films. Chem Solut Depos Funct Oxide Thin Film 2013:1–796. doi:10.1007/978-3-211-99311-8.

[95] Zeng K, Deepankar P, Brent S. A review of thermal analysis methods in Laser Sintering and Selective Laser Melting. Solid Free. Fabr. Symp., 2012, p. 796–814.

[96] Böhmer TS. Enthalpy of fusion prediction for the optimisation of salt based latent heat thermal energy stores. University of Pretoria, 2018.

[97] Wejsa J. ARDEC Energetics. ARDEC Energ. Jt. Armaments Conf., 2010, p. 1–16.

[98] Aluker ED, Krechetov AG, Mitrofanov AY, Zverev AS, Kuklja MM. Understanding limits of the thermal mechanism of laser initiation of energetic materials. J Phys Chem C 2012;116:24482–6. doi:10.1021/jp308633y.

[99] Bardenhagen SG, Luo H, Armstrong RW, Lu H. Detailed characterization of PBX morphology for mesoscale simulations. AIP Conf Proc 2012;1426:637–40. doi:10.1063/1.3686359.

[100] Henry Cohn. Sphere packing 2015:14.

Appendix A

Seed precipitation

Two different seed precipitation method executed to coat the rdx simulant with PCL, 90:10% simulant/polymer mixtures:

i) 450 mg of the coating material (binder) was dissolved in a low boiling organic solvent, followed by dissolution or dispersion. The binder solution containing the core material (simulant particles) was stirred in deionised water containing 1% PVA as a suspension agent and stabiliser. The droplet suspension thus attained was then subjected to solvent evapouration to effect the hardening of the coating material on the simulant particles and thus corresponding microspheres, as shown in Figure 14.

ii) The encapsulation of the simulant particles with PCL was conducted through the use of three solvents, with temperature and pressure conditions varied. The fabrication of the simulant with PCL was achieved with the use of DCM, Chloroform and Cyclohexanone to dissolve a PCL into a solution, according to the protocol described below. Changing the solvents and environment variables was to assess the effect each parameter on the coating and the particle size of the coated material. The expectation from these formulations is that as the solvent evaporates, the PCL will precipitate on the simulant crystals and thereby forming a thin coating and serve as a fabrication between the crystals.

A 450 mg of the simulant powder was suspended in a solution of 20 ml selected solvent (DCM, chloroform and cyclohexanone, separately) containing 50 mg PCL. The mixture was stirred gently between 200-300 rpm for four hours. The solvent was evaporated slowly at different conditions summarised in Table 1.

Dip coating methods

50 mg PCL was dissolved in 10 ml DCM. 450 mg of simulant contained in a sieve was dipped in the binder solution for 10 minutes. The simulant was removed from the binder solution and dipped in 40 ml deionised water for 10 minutes. It was then withdrawn and allowed to drip and dry for about 1 hour.

The same process was followed but with the addition of 1 drop surfynol as a surfactantinto the DCM before dipping the simulant.

Co-precipitation via single emulsion process

A 90%:10% by mass simulant to PCL was formulated. A 450 mg of simulant was suspended into 2 ml PVA 1%w/v. A solution of 50 mg PCL was prepared into 8 ml dichloromethane (DCM) and 2 drops of Surfynol 104-PG50. The latter was emulsified into the kbt solution at 10000 rpm for 3 minutes by using a homogeniser. The first emulsion was homogenised into an already prepared 40 ml PVA 1% for 5 minutes at 20000 rpm to obtain a more stabilised emulsion. The emulsion was spray dried for 45 hours. The powder collected was then weighed and analysed, powder shown in appendix 1. Nanoparticles were formed from this formulation process.

Appendix B

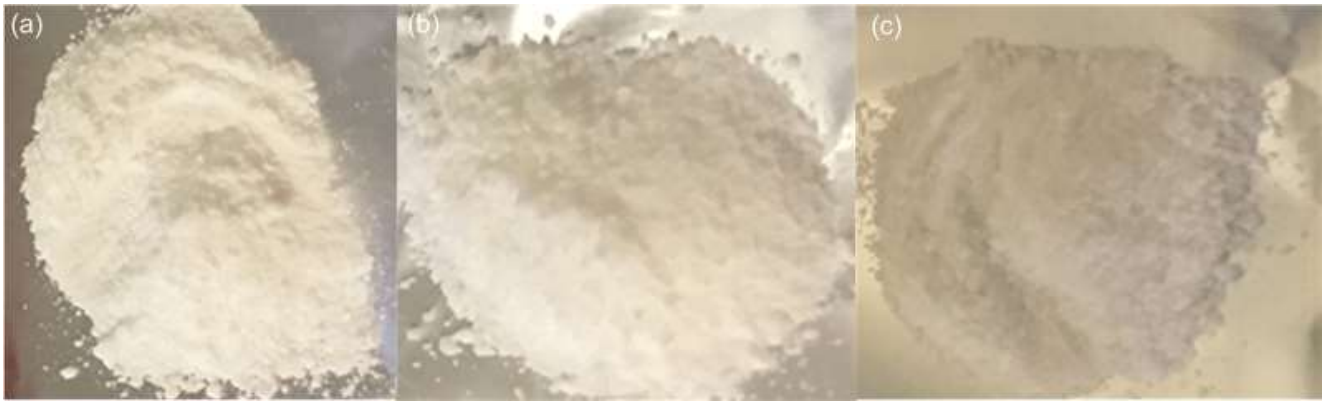

Figure 34: Photos of the mock powder prepared through (a) Seed precipitation, (b) Dip coating, and (c) Co-precipitation.